Effects of riparian vegetation on topographic change during a large flood event, Rio Puerco, New Mexico, USA

M. C. Perignon,[1] G. E. Tucker,[1] E. R. Griffin,[2] and J. M. Friedman[3]

Received 29 July 2012; revised 8 April 2013; accepted 10 April 2013; published 2 July 2013.

[1] The spatial distribution of riparian vegetation can strongly influence the geomorphic evolution of dryland rivers during large floods. We present the results of an airborne lidar differencing study that quantifies the topographic change that occurred along a 12 km reach of the Lower Rio Puerco, New Mexico, during an extreme event in 2006. Extensive erosion of the channel banks took place immediately upstream of the study area, where tamarisk and sandbar willow had been removed. Within the densely vegetated study reach, we measure a net volumetric change of 578,050 $\pm \sim$ 490,000 m^3, with 88.3% of the total aggradation occurring along the floodplain and channel and 76.7% of the erosion focusing on the vertical valley walls. The sediment derived from the devegetated reach deposited within the first 3.6 km of the study area, with depth decaying exponentially with distance downstream. Elsewhere, floodplain sediments were primarily sourced from the erosion of valley walls. Superimposed on this pattern are the effects of vegetation and valley morphology on sediment transport. Sediment thickness is seen to be uniform among sandbar willows and highly variable within tamarisk groves. These reach-scale patterns of sedimentation observed in the lidar differencing likely reflect complex interactions of vegetation, flow, and sediment at the scale of patches to individual plants.

Citation: Perignon, M. C., G. E. Tucker, E. R. Griffin, and J. M. Friedman (2013), Effects of riparian vegetation on topographic change during a large flood event, Rio Puerco, New Mexico, USA, *J. Geophys. Res. Earth Surf.*, *118*, 1193–1209, doi:10.1002/jgrf.20073.

1. Introduction

[2] The morphology of alluvial river corridors is primarily dictated by the interactions of water, sediment, topography, and vegetation during flood events. The influence of riparian vegetation on the dynamics of the flow and the morphology of rivers has been extensively explored [*Hupp and Osterkamp*, 1996; *Micheli and Kirchner*, 2002; *Simon and Collison*, 2002; *Murray and Paola*, 2003; *Corenblit et al.*, 2007; *Tal and Paola*, 2007; *Corenblit and Steiger*, 2009; *Osterkamp and Hupp*, 2010]. Understanding the role that vegetation plays on the evolution of arid and semiarid rivers has been of particular importance given their significant contribution of sediment to the fluvial system [*Tooth*, 2000; *Tooth and Nanson*, 2000; *Coulthard*, 2005; *Hooke*, 2007; *Sandercock et al.*, 2007; *Dunkerley*, 2008; *Stromsoe and Callow*, 2012]. The effects of the invasive species *tamarisk* on the geomorphology of dryland rivers have been of special interest since its introduction to the American southwest in the early 20th century [*Graf*, 1978; *Barz et al.*, 2009; *Pollen-Bankhead and Simon*, 2009; *Vincent et al.*, 2009; *Jaeger and Wohl*, 2011].

[3] The relative importance of the mechanisms that govern morphologic change vary across spatial and temporal scales [*Finnigan*, 2000; *Nepf*, 2012a, 2012b]. At the patch scale, the presence of vegetation on the channel can increase the drag on the flow and reduce the flow velocity [*Raupach*, 1992; *Larsen et al.*, 2009; *Folkard*, 2011], as well as deflect the flow toward zones of bare ground [*Rominger and Nepf*, 2011; *Zong and Nepf*, 2011]. As water interacts with emergent vegetation, large vortices dissipate while turbulence at the scale of the stems increases [*Tanino and Nepf*, 2008]. Where the clusters of vegetation are sparse, this turbulent energy can exceed that of nearby bare beds [*Nepf*, 1999; *Finnigan*, 2000], leading to enhanced erosion [*Moore*, 2004; *Vollmer and Kleinhans*, 2007; *Celik et al.*, 2010; *Lawson et al.*, 2012]. Roots can also increase the stability of banks by boosting their cohesion [*Thorne*, 1990; *Abernethy and Rutherfurd*, 2000; *Simon and Collison*, 2002; *Simon and Thomas*, 2002] and thus raising the threshold for sediment transport. At the reach scale, the drag that plants impart on the flow is thought to be determined primarily by the fraction of the channel cross section that is vegetated [*Green*, 2005; *Nikora et al.*, 2008; *Luhar et al.*, 2008]. The effects that the spatial distribution of vegetation across the landscape have on flow resistance and topographic evolution are still an open question [*Bal et al.*, 2011; *Luhar and Nepf*, 2013].

[1]CIRES and Department of Geological Sciences, University of Colorado, Boulder, Colorado, USA.
[2]U.S. Geological Survey, Boulder, Colorado, USA.
[3]U.S. Geological Survey, Fort Collins, Colorado, USA.

Corresponding author: M. C. Perignon, Department of Geological Sciences, University of Colorado, Campus Box 399, 2200 Colorado Ave., Boulder, CO 80309-0399, USA. (perignon@colorado.edu)

©2013. American Geophysical Union. All Rights Reserved.
2169-9003/13/10.1002/jgrf.20073

[4] The availability of data sets that capture changes in the topography of rivers over time has allowed the application of the morphological method [*Ashmore and Church*, 1998] as an alternative to directly measuring sediment transport. Several techniques have been previously used to collect these repeating data sets, including hand and total station surveys of cross sections [*Milne and Sear*, 1997], real-time kinetic global positioning system (RTK-GPS) [*Brasington et al.*, 2000], aerial photography [*Winterbottom and Gilvear*, 1997; *Lane*, 2003; *Westaway et al.*, 2003], ground-based lidar [*Wheaton et al.*, 2010], and combinations of several methods [*Lane et al.*, 2003].

[5] The collection of multiple airborne lidar data sets allows for the detection of topographic change over large areas of the landscape at higher spatial resolutions than other methods provide. Multitemporal airborne lidar surveys have previously been used to create digital elevation models (DEMs) of Difference (DoDs) that capture geomorphic change in coastal terrain [*Woolard and Colby*, 2002; *White and Wang*, 2003; *Sallenger et al.*, 2004; *Mitasova et al.*, 2009; *Richter et al.*, 2011], glaciers [*Hopkinson and Demuth*, 2006; *Abermann et al.*, 2009], evolving landslides [*Corsini et al.*, 2007; *Burns et al.*, 2010; *Ventura et al.*, 2011; *DeLong et al.*, 2011], volcanic landscapes [*Favalli et al.*, 2010], seismically disturbed watersheds [*Matsuoka et al.*, 2008], and gradually evolving braided rivers [*Wheaton et al.*, 2013]. The stochastic nature of floods has made it difficult to capture the changes resulting from extreme events using this method. So far, it has only been possible to use airborne lidar for fluvial change-detection studies in locations where large events are anticipated [*Procter et al.*, 2010].

[6] We use multitemporal airborne lidar to quantify the spatial patterns of morphologic change that resulted from a large flood on a vegetated reach of a dryland river following the widespread removal of invasive and native plants upstream. This is one of the first case studies that uses multitemporal airborne lidar to capture the morphological changes caused by a large precipitation-driven flood throughout a river corridor. The unique conditions captured at this site make it an ideal natural experiment for understanding the role of floodplain vegetation on the distribution of sediment across the landscape. This case study also explores the consequences of widespread removal of invasive plants on downstream fluvial systems and the potential influence of vegetation on the long-term evolution of arroyos.

2. Field Site

[7] The ephemeral Rio Puerco drains 19,030 km^2 of semiarid north-central New Mexico (NM) in the American southwest (Figure 1, inset). The watershed is dominated by easily eroded fine-grained sedimentary rocks [*Nordin and Curtis*, 1962; *Heath*, 1983; *Love*, 1986], resulting in high sediment discharges of clay, silt, and sand [*Phippen and Wohl*, 2003]. Coarser sediment fractions are seldom found within the arroyo and do not represent a significant component of the sediment load. Streamflow in the Rio Puerco is mostly unregulated. High flows usually result from convective thunderstorms between July and October and have durations ranging from hours to days [*Heath*, 1983; *Griffin et al.*, 2005].

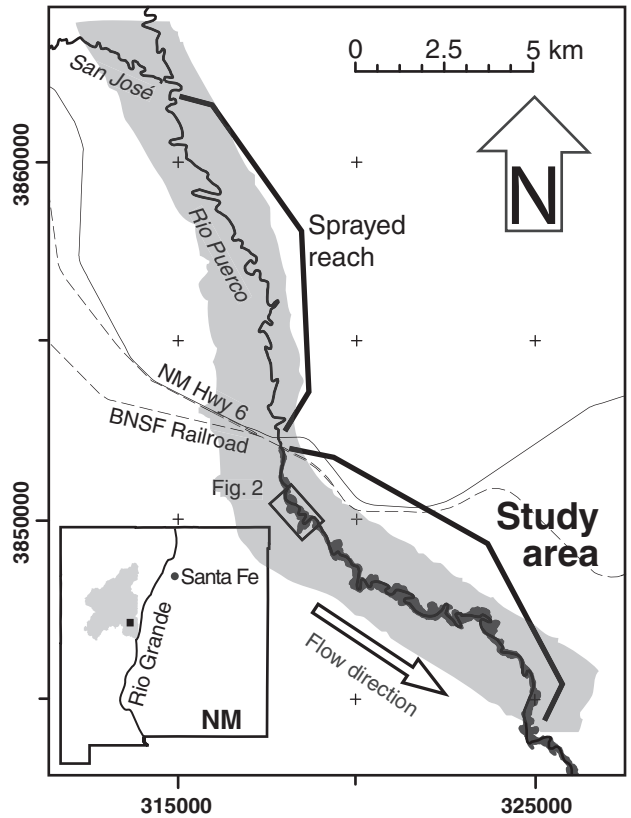

Figure 1. Location map of the area of interest in the Lower Rio Puerco. Light gray shading shows the area covered by the 2010 airborne lidar data set. Dark gray shading shows part of the area of the 2005 lidar data set, which extends for 50 linear kilometer downstream of Highway 6. The study area is the zone of overlap between the two data sets, immediately downstream of the devegetated ("sprayed") reach. Inset map shows the location of the watershed (gray) and study area (black square).

[8] The Rio Puerco, like most arroyos in the American southwest, has gone through cut-and-fill cycles during the late Quaternary [*Karlstrom and Karlstrom*, 1987; *Waters and Haynes*, 2001], with the most recent episode of incision taking place during the late 19th century and early 20th century [*Bryan*, 1925, 1928; *Thornthwaite et al.*, 1942]. The causes and mechanisms of arroyo evolution are debated [*Leopold*, 1976; *Karlstrom and Karlstrom*, 1987; *Elliott et al.*, 1999; *Gellis et al.*, 2001, 2011; *Harvey et al.*, 2011] and are thought to include changes in mean rainfall, precipitation intensity, vegetation or land use, or the crossing of geomorphic thresholds.

[9] During the mid-19th century, most of the Lower Rio Puerco occupied a broad and gentle floodplain that supported irrigation along the valley [*Bryan*, 1928]. By the early 1900s, however, channel incision had created a continuous, steep-walled canyon (arroyo) about 10 m deep, 100 m wide, and 200 km long [*Bryan and Post*, 1927; *Bryan*, 1928; *Elliott et al.*, 1999]. Arroyo incision in the Rio Puerco generated very high sediment loads and caused channel aggradation, avulsion, and flooding along the Middle Rio Grande. The source of the sediment transported by the river has changed as the Rio Puerco has progressed through the arroyo cycle.

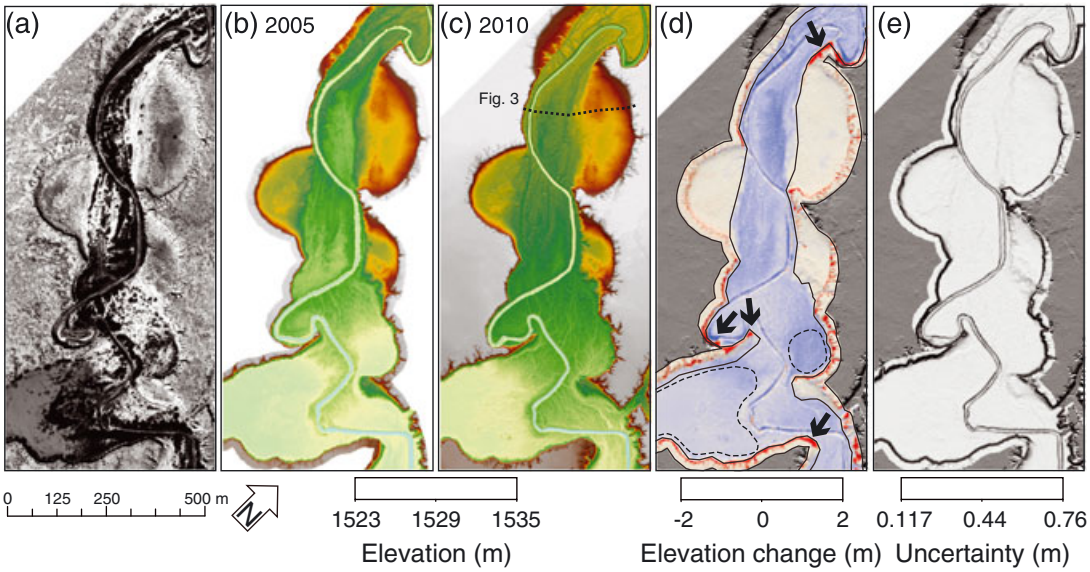

Figure 2. Plan view of the arroyo 2 km down-valley from NM Highway 6 (extent shown in Figure 1). (a) Quickbird II satellite image (panchromatic with 60 cm pixels) collected on 15 November 2006. Darkest areas indicate vegetation. (b) Shaded relief map of 2005 lidar data set, corrected for the systematic error (9.75 cm), with 2 m cells. (c) Shaded relief map of 2010 lidar data set with 0.5 m cells showing the location of the GPS cross section. (d) Lidar differencing calculated by subtracting the corrected 2005 DTM from the 2010 DTM, with 2 m cells. Cool colors show positive topographic change (aggradation), warm colors show negative change (erosion). Solid black lines delineate the arroyo bottom (interior), and walls and terraces (exterior). Dashed black lines approximate the outline of floodplain depressions. Arrows indicate sections of the arroyo wall that collapsed as large blocks. (e) Map of differencing uncertainty (shown over shaded relief map for context), with 2 m cells.

During the early 20th century, material originated almost equally from erosion of the main stem channel and banks, the incising tributaries, and rill erosion of the upper valley surface [*Happ*, 1948]. The source of sediment transported by the river has migrated upstream as the Rio Puerco has progressed through the arroyo cycle [*Happ*, 1948; *Elliott et al.*, 1999]. *Gellis et al.* [2011] calculated that, at present, 80% to 100% of the sediment originates from the erosion of the vertical arroyo walls of the main stem and tributaries.

[10] The sediment that the Rio Puerco supplied to the Middle Rio Grande posed a threat to the Elephant Butte Reservoir, a 2.7 billion m^3 reservoir constructed in 1916. In 1925, the Bureau of Reclamation estimated that sediment largely derived from the Rio Puerco would fill the reservoir by 1980 [*Collins and Ferrari*, 2000]. This prompted the introduction of tamarisk (*Tamarix ramosissima*) in 1926 to the Rio Puerco watershed as a means of erosion control [*Bryan and Post*, 1927]. Since then, tamarisk has become the dominant species in the Lower Rio Puerco. Mature tamarisk are 2 to 8 m tall woody plants with dense branch networks that form linear bands along former levees. Young tamarisk have thin stems and grow in floodplain depressions where overbank flow velocities tend to be slow. The banks of the channel are lined with dense colonies of 1 to 3 m tall native sandbar willow (*Salix exigua*), which have thin and flexible stems. A variety of small shrubs and occasional cottonwood trees also grow on the floodplain and terraces (Figure 2a).

[11] The high density of stems along the channel banks and floodplains exert considerable drag on overbank flow [*Smith and Griffin*, 2002; *Kean and Smith*, 2004; *Smith*, 2007], decreasing the boundary shear stress and reducing erosion within vegetated reaches [*Kean and Smith*, 2004]. The introduction of tamarisk to the Rio Puerco led to more stable banks and attenuated floods, and contributed to dramatic channel narrowing, arroyo filling, and a reduction in the volume of sediment delivered to the Rio Grande [*Vincent et al.*, 2009].

[12] Following its spread along other rivers in the American southwest, tamarisk has become the second most abundant woody riparian plant in the interior western United States [*Elliott et al.*, 1999; *Molnar and Ramirez*, 2001; *Friedman et al.*, 2005]. Tamarisk is a target for control efforts across the western US because it may increase water lost to evapotranspiration and decrease habitat for native species [*Shafroth et al.*, 2005]. The widespread removal of tamarisk from floodplains, however, has been seen to increase erosion [*Pollen-Bankhead and Simon*, 2009; *Vincent et al.*, 2009].

2.1. 2006 Flood of the Lower Rio Puerco

[13] In September 2003, the Valencia Soil and Water Conservation District sprayed the herbicide Imazapyr on the banks and floodplains of a 12 km reach of the Lower Rio Puerco (Figure 1), killing most tamarisk and sandbar willow. Over the next 3 years, minor flows removed some of the woody debris from the banks [*Vincent et al.*, 2009]. Field observations and aerial photographs show that, by 2006, the vegetation density along the sprayed reach was lower than elsewhere in the arroyo.

[14] In August 2006, a period of severe storms caused the largest flood in the Rio Puerco since 1972 [*Vincent et al.*, 2009]. The largest precipitation values for the watershed

were recorded at the National Weather Service climate station in Cubero, NM (station number 292250, 57 km northwest of the Highway 6 bridge), with a total of 163 mm falling mostly before 7 August. The repeated high precipitation resulted in increased discharge at Bernardo, NM, 81 km downstream from the study area, between 4 and 11 August 2006. A peak flow of 176 m^3/s was recorded at Bernardo (U.S. Geological Survey (USGS) streamgage 08353000) at 5:00 AM MST on 10 August 2006 and lasted about 14 h. The discharge across the flooded arroyo bottom at the study reach was not directly measured but was estimated to be 625 m^3/s near the Highway 6 bridge (E. R. Griffin, submitted, 2013).

[15] The 2006 flood caused extensive erosion and channel widening along the devegetated reach (Figure 1). Around 62% of the banks in the sprayed reach eroded, widening the channel from an average width of 12.7 m in 2005 to 23.4 m in November 2006 [*Vincent et al*., 2009; *Griffin et al*., 2010]. This study quantifies the topographic change that occurred along the valley immediately downstream of the sprayed reach.

3. Lidar Differencing for Change Detection

[16] We focus on a 12 km segment of the Rio Puerco immediately downstream of the sprayed reach where healthy vegetation remained on the banks and floodplain at the time of the 2006 flood (Figure 1). Field observations suggest that widespread floodplain sedimentation occurred along this reach, decreasing in thickness with distance downstream of the Highway 6 bridge. Enhanced aggradation is apparent within dense vegetation, while overbank channels are seen to have formed in the bare areas between groves of tamarisk.

[17] Two overlapping high-resolution topographic data sets bracket the 2006 flood event. On 5 April 2005, airborne lidar data were collected for the portion of the arroyo between Highway 6 and Bernardo, NM, near the confluence with the Rio Grande (Figure 2b). A second data set was obtained on 26 March 2010, postdating the flood, that extends from the confluence of Rio Puerco and Rio San Jose, at the upstream end of the devegetated reach, to a point 12 km down-valley from the Highway 6 bridge (Figure 2c). The study area consists of the 3,656,408 m^2 of overlap between the two data sets. By subtracting the elevations of the pre-event lidar-derived digital terrain model (DTM) from those of the post-event DTM, we can measure the topographic change that occurred between the two collection campaigns at every point in this area (Figure 2d). Because the 2006 event was the only major flood that occurred within this time period, we assume that the differencing of the two lidar data sets records the net elevation change that resulted from this flood.

[18] The 2005 lidar data set was collected and processed by Spectrum Mapping LLC. The provided bare ground point cloud (0.91 points/m^2) and DTM (2 m spacing) have a reported horizontal and vertical positional accuracy of 30 cm (Spectrum Mapping LLC, unpublished report, 2005). The National Center for Airborne Laser Mapping (NCALM) collected and processed the 2010 data set. The classified point cloud (6.08 points/m^2) and first-return (unfiltered) and bare-earth DTMs (0.5 m spacing) have a reported vertical accuracy of 5 cm and a horizontal accuracy of 10 cm [*National Center for Airborne Laser Mapping*, 2011].

[19] The 2005 DTM supplied by the contractor showed significant error in the position and slope of the arroyo walls due to imprecisions in the delineation of the slope breaklines. We created a new bare ground DTM with 2 m spacing by interpolating the 2005 bare ground point data using an inverse distance weighted technique with no breaklines. The resulting DTM more accurately represents the position and morphology of the arroyo walls as observed in aerial and satellite imagery. Resampling the 2005 data set into a finer grid led to artifacts along the arroyo walls. The 2010 bare ground and first-return DTMs were therefore aggregated into tiles with 2 m spacing to match the cell size of the 2005 data set. All data sets were clipped to cover the same extent and referenced to the universal time meridian coordinate system, Zone 13N, North American Datum of 1983 (NAD 83). Elevations were referenced to the North American Vertical Datum of 1988 (NAVD 88).

3.1. Calculating and Mapping Uncertainty

[20] For the results of a differencing study to be meaningful, the minimum level of change that is detectable above the noise of the data must be determined [*Brasington et al.*, 2000]. The rapid magnification of error during the creation of derivative products such as differencing maps requires that the uncertainty be determined directly for the derived products [*Burrough and McDonnell*, 1998; *Westaway et al*., 2000; *Wise*, 2000]. In DEM of Difference (DoD) studies, the uncertainty is assumed to be either spatially uniform, constant within zones of similar characteristics [*Westaway et al.*, 2003; *Lane et al.*, 2003] or variable for every cell of the raster [*Wheaton*, 2008]. For this study, the uncertainty of the DEM of Difference will be the sum of errors of four categories: (1) *systematic error* affecting the accuracy of the measurements, (2) *random error* affecting the precision of the data, (3) *filtering error* arising during the extraction of bare ground points from the raw data, and (4) *interpolation error* resulting from the transformation of point data to continuous rasters across complex topography.

3.1.1. Systematic Error

[21] Systematic errors in DEMs of Difference primarily arise from the horizontal (δ_{Sh}) and vertical (δ_{Sv}) misalignment of the elevation data sets [*DeLong et al.*, 2011; *Streutker et al.*, 2011]. When systematic errors can be quantified, a correction can be applied to the position of the data sets to reduce the overall uncertainty of the DoD.

[22] A horizontal shift between the two DTMs can result in significant changes in the patterns of differencing across the landscape. The error will be largest along steep slopes, where horizontal misalignment can result in large apparent vertical shifts. The majority of the techniques used to detect horizontal misalignment [e.g., *Maas*, 2000, 2002; *Kraus et al*., 2006; *Akca*, 2010] are based on a least-squares matching process of nonchanging surfaces where one data set is shifted until the absolute difference between the two is minimized. Other methods that are applied extensively in engineered environments use patch [*Filin*, 2005] or linear feature matching [*Habib et al.*, 2008] and depend on detailed knowledge of the geometry of control surfaces. The lack of multiple well-constrained nonchanging surfaces or artificial structures in the study area make the Rio Puerco DoD a poor candidate for the use of these methods.

[23] *DeLong et al.* [2011] used systematic variations in topographic change with surface slope angle (following *Streutker et al.* [2011]) to calculate the horizontal corrections necessary to co-register two data sets. This method works best if used in large areas with smoothly varying surfaces, a range of slope values and minimal morphologic change between images. We modified this technique for use in the study area by isolating the arroyo walls and observing the values of the DoD across a range of aspects. If the two data sets are misaligned, then large values of positive topographic change are expected along arroyo walls of similar aspect. Using this method, we found no evidence for significant horizontal offset between the two data sets at a scale coarser than the reported positional accuracy.

[24] Any vertical displacement between the 2005 and 2010 DTMs will result in errors in the magnitude of the topographic change measured at every point in the landscape and very large differences in the net volumetric change calculated across the entire DoD. Repeat measurement of the elevation of unchanging surfaces is the most commonly used method for determining the systematic vertical offset between data sets as well as the random noise that is part of the measurement uncertainty [*Lane et al.*, 1994; *Brasington et al.*, 2000; *Wheaton*, 2008; *Mitasova et al.*, 2009; *DeLong et al.*, 2011]. The Highway 6 bridge would seem to serve as an ideal surface to use with this method, but its elevation changed between 2005 and 2010 after it was repaved. Several small rudimentary access roads exist in the study area, but their surface elevation and position cannot be assumed to be unchanging.

[25] The floor of the valley into which the arroyo is incised is a long-term stable flat surface that should have seen minimal net elevation change between the acquisition of the two data sets. Small-scale change, however, is expected to have been caused by overland flow, aeolian processes, and animal activity. The 2005 DTM does not extend far onto the valley floor above the vertical arroyo walls (Figure 2b), limiting the availability of data. The edge of the valley floor along the arroyo walls is actively modified by piping of overland flow through the substrate and by the rotation and collapse of fractured blocks into the arroyo. To remove areas prone to such effects, we defined cells of the valley floor more than 10 m away from the arroyo wall as long-term stable flat surfaces. Terraces within the arroyo, which were not directly impacted by the 2006 flood, also serve as stable vertical references. These surfaces receive sediment from the uplands through overland flow during large storms as well as wind-blown dust throughout the year, and they lose material to the modern floodplain via overland flow, aeolian processes, and surface reworking by grazing cattle. Their net topographic change between 2005 and 2010 is, however, likely very small and focused primarily along the arroyo walls and the edge of the terraces.

[26] In the absence of systematic or random error, the stable surfaces should show no difference in elevation between the 2010 and 2005 DTMs. We find, however, a median difference between the elevation of all cells in these areas of 9.75 cm. This value represents the systematic vertical offset δ_{S_V} between the two data sets for the entire study area. While the misalignment is within the published vertical accuracy of both data sets, it represents 356,450 m^3 of difference over the entire reach. We corrected the vertical position of the 2005 data set by increasing the elevation of all its cells by the systematic error to reduce the median difference between the elevation of the long-term stable surfaces to zero.

3.1.2. Random Error

[27] The noise around the median elevation differences of the cells of the stable surfaces is, in part, caused by the random error that propagates from the point elevation measurements to the DTMs [*Wheaton*, 2008]. The standard deviation for the distribution of elevation differences of the stable surfaces is 11.7 cm. Real changes in the topography of these surfaces between 2005 and 2010 are also captured within this variability. In the absence of fully stable surfaces, it is not possible to isolate the random error that originates from the lidar measurements from these real changes. We therefore assume that the standard deviation of the difference distribution, 11.7 cm, is the total random error δ_R of the DoD. This approach likely overestimates the uncertainty of the DEM of Difference.

3.1.3. Filtering Error

[28] Creating DTMs that reflect the surface topography of the study area requires removing from the raw point data the laser signals that were intercepted by vegetation. Filtering algorithms commonly use four characteristics to classify a point as bare ground: lowest elevation within a buffer area, slope threshold, relief threshold when compared to points around it, and surface smoothness [*Zhang and Whitman*, 2005; *Meng et al.*, 2010]. Few studies have investigated the propagation of terrain filtering error into derivative products such as DEMs of Difference [*Fisher and Tate*, 2006; *Kobler et al.*, 2007]. The accuracy of the filtering algorithms is most commonly tested by comparing the elevation of a bare ground DTM with other high-resolution measurements of the surface [e.g., *Bowen and Waltermire*, 2002; *Hutton and Brazier*, 2012]. We use this approach both as a general validation test of the accuracy of the lidar data and as a means of identifying potential vegetation filtering errors.

3.1.3.1. Lidar Validation Using GPS Survey

[29] A high-precision GPS survey of a section of the study area and the zone immediately upstream of Highway 6 was performed within a week of the collection of the 2010 data set. This survey provides independent data with which to test the validity and accuracy of the lidar DTMs. We classified each GPS point as stable surface, near wall, bare floodplain, or vegetated floodplain using 2006 Quickbird II imagery. Points within the channel, where the GPS elevations record the elevation of the bed but the lidar detected the water surface elevation, were removed. Figure 3 shows the GPS and 2010 bare ground DTM elevations for a cross section of the arroyo (location of the cross section shown in Figure 2c). The difference in elevation between the GPS and 2010 DTM data for points classified as bare floodplain (n = 467) and vegetated floodplain (n = 36) had similar median values (1 cm or less) and standard deviation (0.09 m). The similarity between the standard deviation of this mismatch and the random error of the DoD suggest that the filtering of vegetation from the lidar data added minimal error to the bare ground 2010 DTM.

[30] While no high-precision GPS survey of similar extent and close timing exists for the 2005 data, RTK GPS data obtained in April 2002 can be used to constrain the precision of the lidar elevation measurements within vegetation.

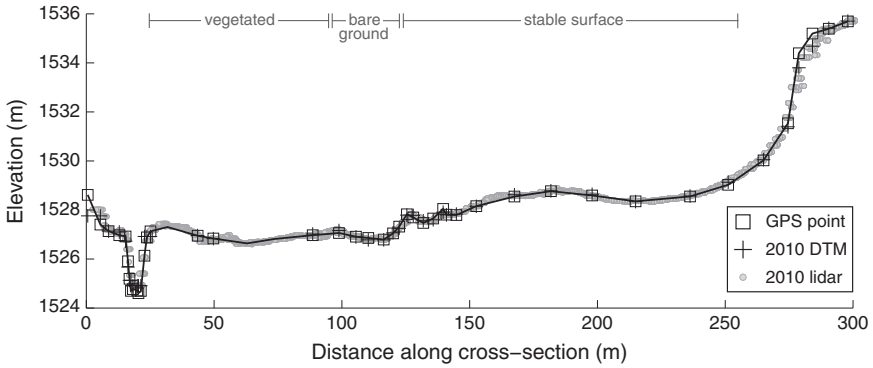

Figure 3. High-resolution GPS elevations collected in early April 2010 (squares) and 2010 DTM elevations at the same locations (crosses). Gray points show the elevation of all bare ground laser returns of the 2010 lidar data set within 2 m of the cross section. There is minimal offset between the elevation of GPS points and DTM within the vegetated and unvegetated arroyo bottom and the stable surfaces, but higher mismatch and spread of the lidar point elevations along the arroyo walls, where the slope is highest.

A total of six point measurements of surface elevation were collected under dense canopy in areas unlikely to have experienced topographic change between 2002 and 2005. The GPS elevation of those points are (median) 0.081 m higher than the elevation at the same location of the uncorrected 2005 DTM (standard deviation of 0.14 m). After correcting the elevation of the 2005 DTM for the systematic error, the median elevation difference becomes 1.6 cm. Given the small size of the sample, the time span between the GPS survey and the lidar campaign, and the similarities between the filtering methods used to process the 2005 and 2010 data sets, we assume that no significant filtering error is introduced to the corrected 2005 DTM by the terrain filtering. A similar analysis by *Vincent et al.* [2009], for a larger area of the Rio Puerco and using the 2005 DTM provided by the contractor, reached similar conclusions.

3.1.4. Interpolation Error

[31] Interpolation errors arise during the creation of DTMs from point data. They can originate from sampling patterns that lead to variability in the point density across the landscape [*MacEachren and Davidson*, 1987], or when the point density is too low to accurately capture the shape of morphologically complex terrain [*Lane et al.*, 2003]. The bare ground points for both the 2005 and 2010 data sets are uniformly distributed across the study area, minimizing the interpolation error of low slope surfaces. Steep slopes, like those along the arroyo walls, can result in large interpolation errors [*Maling*, 1989; *Hodgson and Bresnahan*, 2004; *Zhang and Whitman*, 2005] because small horizontal misplacements of the point measurements of elevation can lead to large shifts in the position of the surface in the interpolated raster. We assume that the interpolation error δ_I for every cell i in each of the Rio Puerco DTMs is primarily a function of the surface slope α_i at that point and the horizontal accuracy of the data $\sigma_{(x,y)}$ for that data set [*Hodgson and Bresnahan*, 2004]:

$$\delta_{I_i} = \tan(\alpha_i)\,\sigma_{(x,y)} \tag{1}$$

[32] The horizontal accuracy of the lidar data is reported by the suppliers as 0.30 m for the 2005 DTM (Spectrum Mapping LLC, unpublished report, 2005) and 0.10 m for the 2010 DTM [*National Center for Airborne Laser Mapping*, 2011].

3.1.5. Creating a Map of Uncertainty

[33] We calculated a final differencing map by subtracting the corrected 2005 DTM from the 2010 DTM to create a raster that represents the topographic change of the landscape between 2005 and 2010. Positive values correspond to upward movement of the surface or net aggradation, while negative numbers show lowering of the surface or net erosion (Figure 2d).

[34] The total uncertainty of the differencing measurements δ_T, for every cell, is equal to [*Brasington et al.*, 2000]:

$$\delta_T = \sqrt{{\delta_R}^2 + {\delta_{I2005}}^2 + {\delta_{I2010}}^2} \tag{2}$$

where δ_R is the random error, and δ_{I2005} and δ_{I2010} are the interpolation errors for the 2005 and 2010 data sets, respectively (Figure 2e). After correcting the elevation of the 2005 DTM, the systematic error δ_{Sv} does not contribute to the total differencing uncertainty.

3.1.6. Field Validation of Differencing Map

[35] The accuracy of the differencing map was tested by measuring the thickness of the 2006 flood deposits in the field on 4–6 November 2011. The material deposited by the 2006 event is primarily fine white sand, in contrast to the often dark red mixture of sand, silt, and clay that covered the floodplain prior to the flood [*Vincent et al.*, 2009]. We dug 26 pits along the first 3.5 km of the floodplain downstream of the Highway 6 bridge and used the appearance of thick clay layers, dark or red sand, or significant oxidation to define the base of the 2006 deposits. The location of each of the pits was selected to be representative of the area and to avoid the effects of small-scale topography and individual plants on the sediment thickness. The coordinates for each pit were collected using a handheld Garmin GPS with a reported accuracy of 15 m (Figure 4).

3.2. Detection of Vegetation

[36] A vegetation map of the study area was generated from remote sensing imagery by classifying each pixel as covered by large woody vegetation, small woody vegetation,

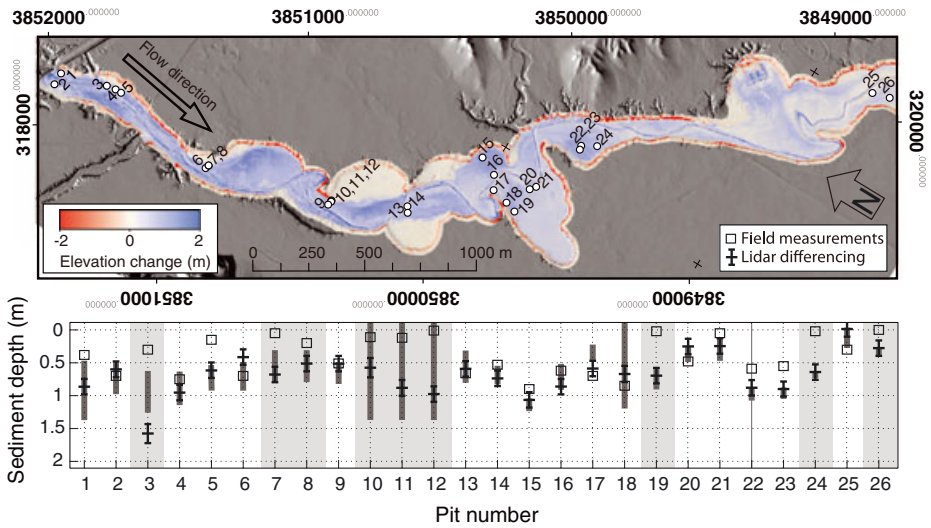

Figure 4. (top) Location of 26 pits where the thickness of the 2006 flood deposits was estimated, and lidar differencing map. NM Highway 6 is seen on the left side of the map. (bottom) Field measurements (squares) and lidar differencing results (crosses, spanning the uncertainty) at every pit location; light gray shading marks sites where the surface deposits are clay rich. Dark gray bars span one standard deviation of the lidar differencing measurements within a 15 m radius around every pit.

or bare ground. The category of large woody vegetation is assigned to zones where the terrain filtering algorithms used to process the 2010 lidar data set detected obstacles above the bare ground. We assume that these areas are vegetated primarily by mature tamarisk, which have dense branch networks that intercept the laser beams before they reach the bare ground. Young tamarisk plants and sandbar willow are effectively invisible to airborne lidar because their thin near-vertical stems and branches do not consistently reflect the laser signals. A minimum height for obstacles of 0.1 m above the surface was selected to remove the random error in the data.

[37] The distribution of plants on the landscape was also mapped from the 2006 Quickbird II images by using an iso cluster unsupervised classification algorithm [*Richards*, 1986] to categorize each pixel as either bare ground or vegetation. Cells classified as vegetated using this method but not by the 2010 lidar were categorized as small woody vegetation. These zones are thought to represent dense groves of sandbar willow and young tamarisk.

[38] Vegetation cover and density were assumed to be constant between 2005 and 2010. The vegetation classification was confirmed to be accurate over this time period by comparing the vegetation map against aerial and satellite imagery, GPS-referenced field photographs of the area surrounding each of the field-validation pits, and overview photographs of the arroyo taken from the Highway 6 bridge and the upper valley surface with identifiable morphological landmarks. The vegetation map was found to accurately detect the patterns of vegetation on the landscape as well as correctly represent the dominant plant type.

3.3. Data Analysis

[39] Separate calculations of topographic change were performed for zones directly impacted by the 2006 flood (arroyo bottom, consisting of the channel and floodplain) and for those outside of its direct path (arroyo walls, terraces, and upper valley surface). The boundary between the near-horizontal arroyo bottom and the steeply sloping walls was delineated automatically by selecting cells of the 2005 DTM with a 6° slope, which are generally found at the toe of the walls. The edges of terraces were selected from the same data set by following zones of high topographic curvature. Both edges were combined and compared to the 2005 DTM for misplacement (Figure 2d).

[40] The coordinate system of the differencing and vegetation maps was transformed to a valley-wise and valley-normal coordinate system using the techniques presented by *Legleiter and Kyriakidis* [2006]. All locations are identified in terms of distance downstream of the Highway 6 bridge along the valley centerline (Figure 5).

[41] Trends of mean topographic change were calculated by averaging the data across 25 m wide slices in the down-valley direction. The spatial correlation between topographic change and vegetation was observed by dividing the DoD and the vegetation map into 25 m by 25 m windows and averaging the values within each cell. The relationship between sedimentation and vegetation was only analyzed for cells within the arroyo bottom along the downstream-most 7 km of the study area, where sediment thickness does not appear to be strongly affected by proximity to the sprayed reach or arroyo morphology. The uncertainties of the differencing measurements are reported as the sum of the uncertainties calculated for each of the cells of the DoD (Figure 2e).

3.4. Results

[42] Figure 6 shows the areal and volumetric distributions of topographic change for the study area, the arroyo bottom, and the walls and terraces. Areal change distributions are histograms that record the total surface area that experienced a given magnitude of change. Volumetric distributions are derived from the areal distributions by multiplying each

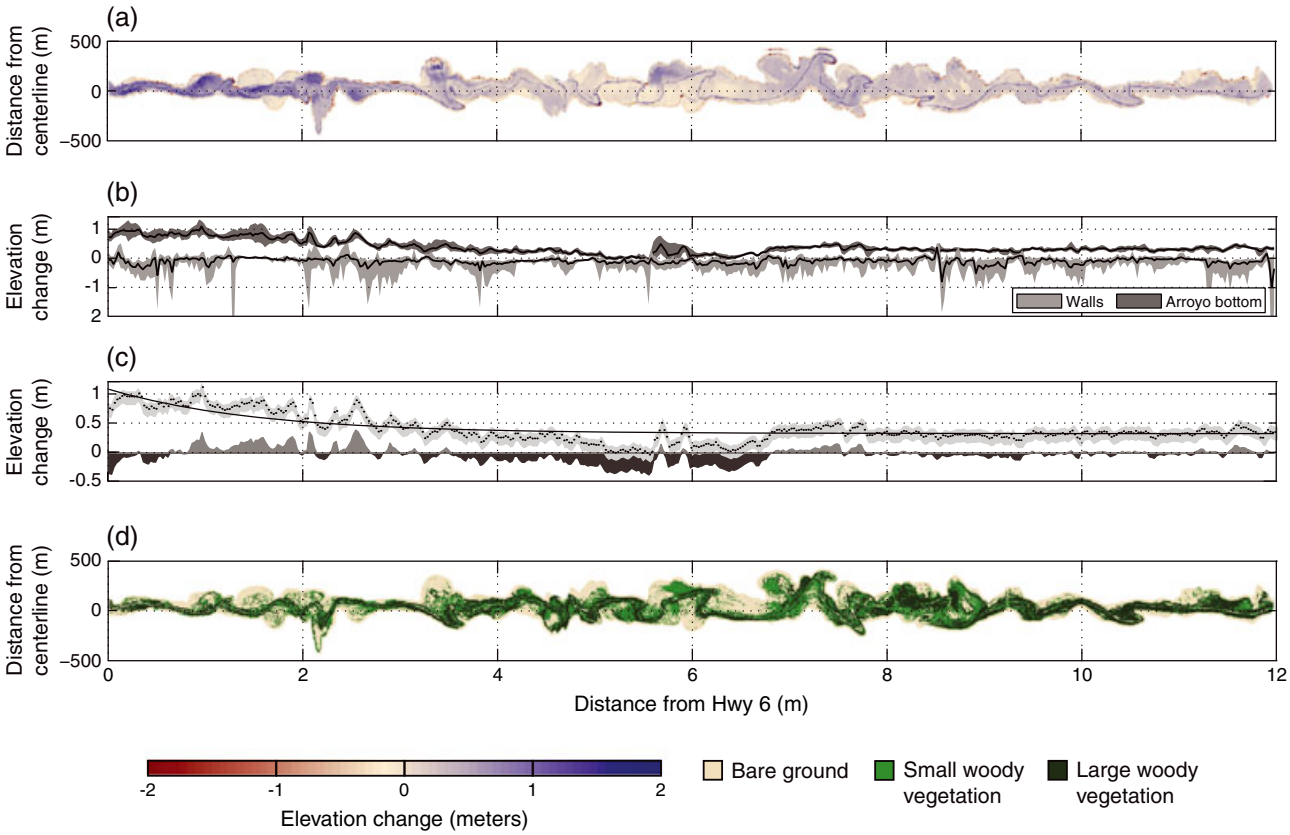

Figure 5. (a) Planform view of the DEM of Difference, in valley-wise and valley-normal coordinates. (b) Quantiles of differencing values within the arroyo bottom (dark gray) and walls (light gray) averaged over 25 m wide windows perpendicular to the valley-wise direction: median (black line) and 25th–75th quantiles (shading). (c) Mean elevation change (black points), uncertainty in the differencing (light gray shading) and theoretical model for sedimentation depth with distance from the sediment source (black line) as shown in equation (8). Deviations of the mean elevation change from the model: overpredictions in dark gray, under-predictions in light gray. (d) Vegetation map created from the difference between the first-stop and bare ground 2010 DTMs (large woody vegetation, dark green) and the iso cluster unsupervised classification algorithm (small woody vegetation, light green).

magnitude of elevation change by the corresponding area [*Wheaton et al.*, 2010].

[43] Table 1 summarizes the average topographic change and measurement uncertainty calculated from the DEM of Difference for each zone of the reach. The differencing map records a net volume change for the study area of 578,050 $m^3 \pm \sim 490{,}000$ m^3, with a mean increase in elevation of 0.16 m ± 0.13 m. The total volume of aggradation measured in the study area is 988,790 $m^3 \pm \sim 330{,}000$ m^3. The elevation of cells showing positive topographic change increased, on average, by 0.37 m ± 0.12 m between 2005 and 2010. Most of the positive topographic change is seen within the arroyo bottom (88.3% of the total volume of aggradation).

[44] A volume of 410,740 $m^3 \pm \sim$ ~~15~~0,000 m^3 is measured as having eroded from the study area, with a mean change in elevation of the eroded zones of –0.42 m ±~~0~~.16 m. Most of the erosion is found along the vertical arroyo walls and terraces, accounting for 76.7% of the total material removed. Gullies and collapsed piping features along the arroyo walls are seen in the lidar differencing as linear zones of negative topographic change on the upper valley surface, perpendicular to the arroyo walls (Figure 2d). Only 2.9% of the study area records more than 1 m of erosion, but this fraction corresponds to 58.4% of the total material eroded. These are sites where blocks, estimated in the field to be around 1.5 m thick, 5 m wide, and the height of the wall, collapsed into the arroyo (shown with arrows in Figure 2d). The differencing map shows that they are found either directly in the path of the down-valley flood flow, facing upstream, or are found where a meander bend abuts the arroyo wall. Zones of focused aggradation are sometimes visible next to sites of high erosion, indicating the growth of point bars or the presence of collapsed blocks within the arroyo bottom.

[45] Field measurements of the thickness of the 2006 flood deposits collected in areas where the surface sediments consisted of medium and fine sands are consistent with the findings of the lidar differencing (Figure 4, no shading), and underestimate the DoD measurements in pits with surface material composed primarily of clays and silty clays (Figure 4, gray shading). In sand-rich pits, the field measurements are on average 0.07 m shallower (standard deviation of 0.26 m) than the local value of the lidar differencing.

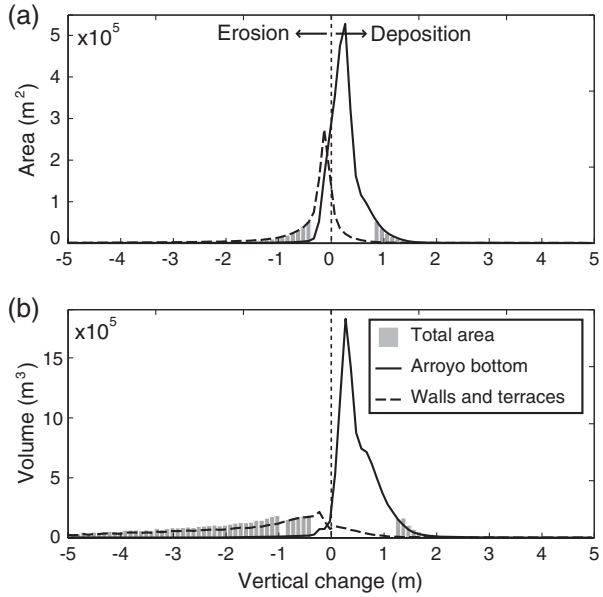

Figure 6. (a) Areal and (b) volumetric differencing distributions for the total study area (gray bars), arroyo bottom (solid line), and walls and terraces (dashed line).

At clay-rich sites, the field measurements are, on average, 0.66 m shallower (standard deviation of 0.31 m) than the values of the lidar differencing.

[46] The vegetation density map shows that plant groves are densest on the banks of the channel and along strips on the inside of meander bends (Figure 5d). The fraction of the floodplain that is blocked by vegetation, known as the blockage factor [*Green*, 2005; *Luhar et al.*, 2008], increases gradually for the first 4 km downstream of Highway 6, with similar proportions of vegetation classified as small woody vegetation and large woody vegetation. Vegetation cover is variable between 4 and 6.5 km and then is uniformly high to the end of the study reach. The floodplain is dominated by small woody vegetation between 4 km and 9.5 km and by large woody vegetation between 9.5 km and the downstream end of the study area.

[47] Figure 7 shows the relationship between mean sediment depth and vegetation density and type for the down-valley 7 km of the study area. There is a poor correlation between mean deposit thickness and vegetation cover, although aggradation is lower in areas with minimal vegetation and generally higher where the landscape is 60–70% covered by vegetation (Figure 7a). A stronger relationship is seen between vegetation density and type and the variability in deposit thickness (Figure 7b). Sites dominated by large woody vegetation show very high variability in sediment depth. Where the landscape is covered by small woody vegetation, sediment depths tend to be uniform across the landscape.

[48] The magnitude and down-valley patterns of topographic change seen in the landscape are different for the arroyo bottom and the walls and terraces (Figure 5b). The mean elevation change recorded within the arroyo bottom is highest immediately downstream of the Highway 6 bridge and decreases with distance down-valley. Downstream of 7 km, the thickness of deposition along the arroyo bottom no longer varies and has a median value of around 30 cm. Along the arroyo walls and terraces, erosion is uniform with distance down-valley for the length of the study area, with a mean value of around 30 cm. Large negative deviations from the mean correspond to zones of localized wall retreat.

4. Theoretical Depositional Profile With Distance From Sediment Source

[49] We aim to determine whether a simple, one-dimensional mass balance model can account for the major down-valley patterns of deposition seen within the arroyo bottom in the lidar differencing. This model does not attempt to fully describe sediment transport along the Rio Puerco during the 2006 flood but instead separates the first-order controls on sediment distribution, such as the distance from the sprayed reach, from the local influence of vegetation and arroyo morphology on the patterns of floodplain aggradation. The model starts with an equation for conservation of suspended sediment:

$$\frac{dCh}{dt} = \dot{E} + \dot{S} - \dot{D} - \frac{dq_s}{dx} \tag{3}$$

Table 1. Total Topographic Change Measured by Lidar Differencing

	Volumetric Change	Mean Elevation Change	% of Zone	% of Change
		Total Area		
Net change	578,050 ± 488,190 m^3	0.16 ± 0.13 m		
Aggradation	988,790 ± 334,400 m^3	0.37 ± 0.12 m	73.5%	
Erosion	–410, 740 ± 153,780 m^3	–0.42 ± 0.16 m	26.5%	
		Arroyo Bottom[a]		
Net change	899,723 ± 316,110 m^3	0.34 ± 0.12 m		
Aggradation	927,300 ± 287,180 m^3	0.39 ± 0.12 m	91.3%	88.3%
Erosion	–27, 577 ± 28,935 m^3	–0.12 ± 0.13 m	8.7%	23.3%
		Walls and Terraces[b]		
Net change	–321, 662 ± 172,070 m^3	–0.30 ± 0.16 m		
Aggradation	61,498 ± 47,224 m^3	0.20 ± 0.15 m	29.8%	11.7%
Erosion	–383, 160 ± 124,850 m^3	–0.52 ± 0.17 m	70.2%	76.7%

[a]71.0% of arroyo area (channel and floodplain).
[b]29.0% of arroyo area (upper valley surface, vertical arroyo walls, and terraces).

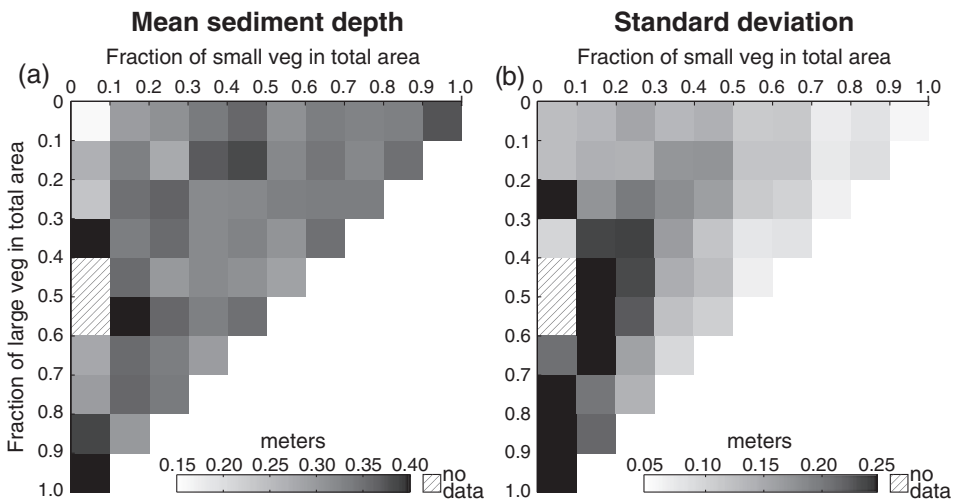

Figure 7. Moving window comparison between lidar differencing values and vegetation density and type within the arroyo bottom between 7 km and 12 km down-valley from NM Highway 6. (a) Mean sediment depth against fraction of small woody vegetation (horizontal axis) and large woody vegetation (vertical axis). Dark colors represent higher depths of sedimentation. (b) Standard deviation of the sediment depth against fraction of small woody vegetation and large woody vegetation in the landscape. Dark colors represent higher variability in sediment depth.

where C is the volumetric sediment concentration in the flow, h is the flow depth, $\dot{E}$ and $\dot{D}$ are the entrainment and depositional fluxes, $\dot{S}$ is the flux of material into the flow from sources other than the bed, q_s is the sediment discharge per unit width, and x is the distance along the valley axis, increasing downstream. The entrainment flux, $\dot{E}$, should depend primarily on the shear stress applied by the flow on the bed. Since the volume of erosion that might have occurred along the arroyo bottom is likely very small relative to the measured volumes of aggradation, we assume that this term is negligible. Assuming steady state sediment concentration in the flow, we can write

$$\frac{dq_s}{dx} = \dot{S} - \dot{D} \tag{4}$$

[50] Many relationships have been proposed to describe the rate of material flux from the flow onto the bed. We assume that the depositional flux is given by the relation $\dot{D} = pv_sC$, where p is a dimensionless number that reflects the distribution of sediment in the water column [e.g., *Davy and Lague*, 2009] and v_s is the net settling velocity of a particle in the flow. The sediment discharge per unit width is given by $q_s = Cq$, where q is the water discharge per unit width. By assuming that the discharge per unit width is uniform with distance downstream, we can write

$$\frac{dC}{dx} = \frac{\dot{S}}{q} - \frac{pv_sC}{q} \tag{5}$$

[51] Integrating with respect to distance, we find an expression for the volumetric sediment concentration with distance downstream from the sediment source.

$$C(x) = \left(C_o - \frac{\dot{S}}{pv_s}\right)\left(e^{-\frac{pv_sx}{q}} + \frac{\dot{S}}{pv_s}\right) \tag{6}$$

where C_o is the sediment concentration at the inlet.

[52] The rate of change of bed elevation $\eta\psi$ is given by the simple relationship

$$\frac{d\eta\psi}{dt} = \frac{\dot{D} - \dot{E}}{1 - \phi\psi} \tag{7}$$

where $\phi\psi$ is the bed porosity. We again consider the erosion rate $\dot{E}$ to be negligible. Combining equations (7) and (6) and integrating over the flood duration t, we can write an expression for the change in the elevation of the channel bed and floodplains:

$$\eta(x,t) = \left(C_o - \frac{\dot{S}}{pv_s}\right)\left(e^{-\frac{pv_sx}{q}} + \frac{\dot{S}}{pv_s}\right)\left(\frac{pv_st}{1 - \phi\psi}\right) \tag{8}$$

[53] This expression suggests that the depth of sedimentation at any point in the study reach can be represented as the sum of the accumulation of material sourced from the sprayed reach, which follows an exponential profile decreasing with distance downstream, and the deposition of sediment that originates from local sources.

[54] We interpret the deviations of the median sediment thickness obtained from the lidar differencing from this theoretical model as reflecting the influence of arroyo morphology and floodplain vegetation on sediment transport. To isolate these processes, we fit the one-dimensional model to the values of median sediment thickness with distance downstream obtained from the DoD. We assume a uniform distribution of sediment in the water column (implying $p = 1$) [*Nordin*, 1963] and a porosity of the sediment on the bed of 30% ($\phi\psi = 0.3$) [*Beard and Weyl*, 1973]. We choose a time $t = 50400$ s to represent the duration of the peak discharge at the Bernardo, NM, streamgage (14 h) and a grain size of 0.045 mm (coarse silt) as representative of the material carried by the flow [*Nordin*, 1963]. Using the formulation of *Ferguson and Church* [2004], which is valid for both viscous and turbulent conditions, we calculate a settling velocity for quartz grains in the flow of $v_s = 0.00175$ ms^{-1}.

[55] We calculate a value for the water discharge per unit width of the arroyo bottom, q, from a total discharge at the Highway 6 bridge of $Q = 625\ \mathrm{m^3\ s^{-1}}$ (E. R. Griffin, submitted, 2013) and a mean width of the active flow equal to the mean width of the arroyo bottom along the study reach $b = 235$ m. This results in a discharge per unit width for the 2006 flood of approximately $q = 2.66\ \mathrm{m^2\ s^{-1}}$.

[56] In the downstream-most 5 km of the study reach, we observe a depositional profile that is essentially uniform in space. This is consistent with the prediction of equation (8) that sediment accumulation should asymptote downstream to a constant depth that reflects local sources. The flux of sediment from sources other than the bed $\dot{S}$ can be calculated from the mean elevation change of the arroyo bottom seen in the lidar differencing downstream of 7 km, $\Delta z = 0.31$ m, to find $\dot{S} = 4.3 \times 10^{-6}\ \mathrm{ms^{-1}}$.

[57] We fit this theoretical model to the down-valley mean values of elevation change (Figure 5b), excluding the data upstream of 1 km and between 5 km and 7 km, to find a value for the incoming sediment concentration C_o. Along those reaches, the local morphology of the arroyo appears to strongly influence the sedimentation pattern. We find that the sediment concentration at the upstream end of the study reach is approximately $C_o = 0.009$ ($R^2 = 0.65$). Figure 5c shows the fit of the theoretical model to the median sediment thickness as well as the deviations of the data from the model.

5. Discussion

5.1. Sources of Sediment Throughout the Rio Puerco

[58] Within the study area, we interpret the down-valley sedimentation pattern as the sum of a depositional profile of the sediment derived from the sprayed reach, which decreases roughly exponentially with distance downstream, and a constant accumulation of material sourced from the arroyo walls and upper valley surface. This interpretation is consistent with a simple one-dimensional mass balance model, which predicts that the contribution of the upstream source should decay exponentially downstream. Below a certain distance downstream of the sediment source, the contribution of sediment from the upstream source is no longer significant, and a balance is reached between the rate of deposition onto the floodplain $\dot{D}$ and the flux of material from external sources $\dot{S}$. For the study reach, we observe a transition about 3.6 km from Highway 6, downstream of which the thickness of the deposits as predicted by the model decreases by less than 0.05 mm per meter downstream. This one-dimensional model therefore suggests that, while the widespread removal of vegetation from the floodplain and banks of the Rio Puerco had significant local consequences for the morphology of the arroyo, its effects outside of the sprayed reach were limited to a zone that extended a little over 3 km downstream.

[59] The extensive bank erosion that occurred along the sprayed reach during the 2006 flood is not found elsewhere along the Rio Puerco. The presence of healthy vegetation along the channel banks and floodplains might have prevented erosion during the 2006 flood by increasing bank stability [*Afzalimehr and Dey*, 2009; *Pollen-Bankhead and Simon*, 2009] and reducing near-bed flow velocity and turbulence [*López and García*, 1998; *Siniscalchi et al.*, 2012].

[60] Localized retreat of the arroyo walls through block collapse is observed to have occurred within the vegetated study area (Figure 2d) as well as throughout the sprayed reach upstream. Erosion of the walls and the edges of the terraces occurred through three distinct processes: (1) piping and gullying by overland flow draining the upper valley surface, (2) the collapse of blocks fracturing parallel to the wall edge, not driven by undercutting, and (3) the failure of large blocks where a meander bend undercuts the arroyo wall. While the first two processes are independent of vegetation and should only be a function of overland flow and soil saturation [*Istanbulluoglu et al.*, 2005], the removal of plants from the floodplain and banks might have led to more effective undercutting of arroyo walls by leaving the banks unshielded and allowing for faster migration of meanders. We are not able to fully quantify the differences in wall erosion between the sprayed and vegetated reaches due to the lack of repeat topography along the upstream section. A visual comparison of the 2005 New Mexico Digital Orthophoto Quarter-Quads (DOQQs) (1 m pixels, collected in July/August 2005) [*New Mexico Geospatial Data Acquisition Committee*, 2006] and the 2010 lidar DTM, however, suggests that the number of large block failures along the arroyo walls is similar between the two reaches.

5.2. Role of Vegetation on Sediment Distribution

[61] Superimposed on the depositional profile described by the one-dimensional mass balance model are the finer-scale effects of arroyo morphology and floodplain vegetation on the distribution of flow and sediment across the landscape. It is not the purpose of this paper to understand the specific mechanisms that governed the interaction of flow, sediment, and vegetation during the 2006 flood (E. R. Griffin, submitted, 2013), but instead to use the patterns of topographic change observed in the lidar differencing to explore the reach- and patch-scale variability in sediment transport across the vegetated landscape.

[62] Two sections of the arroyo show major deviations from the predicted profile. In the reach that extends 0.75 km downstream from Highway 6, the depth of sedimentation is lower than predicted by equation (8). We speculate that the presence of the Highway 6 bridge prevents the free movement of the channel across the floodplain, forcing the arroyo to remain narrow and leading to higher flow velocities that limit deposition. The steep channel gradient under the bridge might also locally increase the flow velocity and contribute to this pattern. The theoretical model is also a poor fit between 3.5 km and 6.8 km down-valley of Highway 6. The upstream end of this section corresponds to an abrupt increase in the width of the arroyo bottom. At around 6.8 km, a broad floodplain depression, previously occupied by a large meander bend but now abandoned, lies isolated from the down-valley flow. The sudden increase in median sediment depth at this location may reflect the accumulation of sediment in this low area. Figure 2d (dashed lines) shows two similar depressions at a different location in the study area that also accumulated material during the 2006 flood.

[63] The presence of vegetation on the landscape is known to create drag and affect the velocity of the flow, the scale and intensity of turbulence [*Raupach*, 1992; *Tanino and*

Nepf, 2008; *Larsen et al.*, 2009; *Folkard*, 2011], and the patterns of shear stress on the bed [*Hopkinson and Wynn*, 2009; *Schoneboom et al.*, 2010]. The drag force exerted by arrays of vertical stems is controlled by stem diameter and spacing. *Griffin et al.* [2005] report that the dense groves of sandbar willow and young, thin tamarisk (here classified as small woody vegetation) on the banks of the Rio Puerco have an average stem diameter D_s of 0.02 m and a stem spacing $\lambda\psi$ of 0.13 m, while the dense forests of large tamarisk (here large woody vegetation) have D_s = 0.20 m stems spaced $\lambda\psi$ = 0.41 m apart. These measurements were collected at a height of 30 cm above the surface to more accurately describe the plant morphology that interacts with overbank flow. The frontal area per unit volume D_s/λ^2 is similar for both classes of vegetation, suggesting that they impart similar amounts of drag on the flow [*Kean and Smith*, 2004]. If the magnitude of sedimentation is only a function of drag, then the depth of the 2006 sediments should increase with increasing plant cover to reach a maximum depth where the floodplains are 100% vegetated. Instead, a weak relationship is seen between sedimentation depth, vegetation type and density (Figure 7a). The lack of a strong correlation indicates that other factors such as flow depth, velocity, and proximity to a local sediment source might significantly contribute to the spatial distribution of sediment along the study reach.

[64] A stronger correlation is seen between the variability in sediment depth across the landscape and vegetation type and cover (Figure 7b) that suggests that the characteristics of vegetation are not only modifying the mean velocity of the flow but are also influencing the spatial distribution of sediment at the patch scale. The presence of vegetation in the path of the flow affects turbulence by breaking up large eddies and producing turbulence at the scale of the stems and their spacing [*Kean and Smith*, 2006; *Tanino and Nepf*, 2008]. There is, however, a nonlinear relationship between stem density and kinetic energy in the flow [*Nepf*, 1999]. When compared to unvegetated landscapes, the flow over reaches with sparse vegetation exhibits augmented turbulence intensity [*Finnigan*, 2000], increasing the variability of deposit thickness and potentially causing erosion [*Moore*, 2004; *Vollmer and Kleinhans*, 2007; *Celik et al.*, 2010; *Lawson et al.*, 2012]. The high variability in sediment depth in areas of the landscape that are dominated by mature tamarisk, with widely spaced thick trunks in wide bands parallel to the channel, could potentially be explained by this process. As the density of stems on the landscape continues to increase, the wakes of individual stems interact more strongly and the intensity of turbulence decreases [*Raupach*, 1992; *Nepf*, 1999; *Larsen et al.*, 2009; *Folkard*, 2011]. Areas of uniform, dense vegetation like those covered by closely spaced sandbar willows could therefore experience slow, uniform flow that results in minimal variability in the depth of sedimentation. Smaller-scale variability in sediment distribution generated by flow structures near the leading and trailing edges of vegetation patches and in the gaps between them [*Sukhodolov and Sukhodolova*, 2010; *Zong and Nepf*, 2010; *Folkard*, 2011; *Siniscalchi et al.*, 2012] cannot be detected at the spatial scale of this case study.

[65] The influence of plant morphology, density, and distribution on the large-scale patterns of flow routing and sedimentation on the landscape is still an unresolved issue [*Bal et al.*, 2011; *Nepf*, 2012b; *Luhar and Nepf*, 2013]. This study suggests that the reach-scale patterns of sedimentation observed through lidar differencing likely reflect complex interactions of vegetation, flow, and sediment at the scale of patches to individual plants.

5.3. Implications for the Evolution of Arroyo Morphology

[66] Extensive bank erosion during the 2006 flood only occurred along the 12 km reach upstream of the study area, where most of the vegetation had been removed [*Vincent et al.*, 2009]. Our theoretical model suggests that the influence of this large sediment source on the morphology of the river corridor downstream is limited to the first 3.6 km of the reach. Downstream of this point, and elsewhere along the arroyo, the sediment that accumulated on the floodplain is sourced primarily from the localized collapse and gullying of arroyo walls. While wall collapse might have been enhanced by increased undercutting in areas void of plants, these processes are active independent of vegetation cover.

[67] It is not possible to close the sediment budget for the sprayed and study reaches of the Rio Puerco because the flux of material from the upper valley surface into the arroyo and the rate of transport of sediment into the sprayed reach and out of the study area cannot be measured. The measurements of volumetric change obtained from the lidar differencing, however, can be combined with estimates of the sediment yield from the sprayed reach to test the hypothesis that the influence of the sediment released from the sprayed reach was limited to the zone immediately downstream. The calculations of volumetric change within the sprayed reach of *Vincent et al.* [2009], however, are not as well constrained as those presented here due to a lack of detailed before-and-after topographic data.

[68] *Vincent et al.* [2009] estimated that 680,000 m^3 of material eroded from the arroyo bottom along the sprayed reach of the Rio Puerco during the 2006 flood, primarily through channel widening. Additionally, we estimate that around 56,000 m^3 of sediment were removed from the arroyo walls along the sprayed reach based on the comparison of the 2005 DOQQs [*New Mexico Geospatial Data Acquisition Committee*, 2006] and 2010 lidar DTM. When combined with the measurements of erosion obtained from the lidar differencing, the total volume of material eroded from the sprayed reach and the study area is approximately 1,150,000 m^3.

[69] Roughly 500,000 m^3 of sediment accumulated on the floodplains of the sprayed reach during the flood [*Vincent et al.*, 2009]. Combined with our calculation of the volume of aggradation seen in the study area, a total volume of aggradation of approximately 1,500,000 m^3 could have occurred among the two reaches.

[70] The estimates of erosion from the sprayed reach and study area account for around 77% of the volume of aggradation over the same area. These calculations ignore possible sources of sediment from the upper valley surface that could contribute large volumes of sediment to the arroyo. *Phippen and Wohl* [2003] measured the volume of sediment behind 17 intact retention dams on the upper valley surface of the Rio Puerco and estimated that each drainage supplies between 104.1 and 4119.8 metric tons of sediment

per year to the arroyo. While these values are small compared to the volume of sediment eroded from the walls of the arroyo, numerous small basins drain into the sprayed reach and study area from the upper valley surface. Several small tributaries also join the main stem along this section that could have contributed significant volumes of material to the flow. Likewise, our estimates of wall erosion along the sprayed reach only include large areas of wall collapse and ignore erosion of the arroyo walls by piping, gullying, and smaller collapses that is seen in the lidar differencing to be prevalent throughout the study reach. It is therefore likely that the material eroded from the sprayed reach because of the removal of vegetation deposited entirely along the arroyo bottom of the sprayed reach and the study area. This implies that arroyo devegetation, at least within the specific fluvial system of the Lower Rio Puerco, does not cause spatially extensive geomorphic change to the riparian corridor downstream.

[71] *Gellis et al.* [2011] argued that, during the initial periods of arroyo filling, material from the walls and upper valley surface accumulates within the incised arroyo, gradually increasing its elevation. We calculate that 76.7% of the sediment that eroded from the study area originated from the arroyo walls and terraces. These findings agree with their measurements at two other sites in the Rio Puerco watershed where 80–100% of the material mobilized is sourced from the arroyo walls. In the Lower Rio Puerco, the erosion of material from the vertical walls of the arroyo is, at least in the short term, independent of the presence of vegetation along the arroyo bottom. The widespread distribution of dense groves of invasive plants along the floodplain and channel within the study area might, however, be accelerating arroyo filling by capturing a large portion of the sediment that is transported during overbank flows.

5.4. Uncertainty in the Measurements of Change

[72] We found large uncertainties associated with the differencing measurements that are a result of random error propagating from the original data as well as vertical error arising from the horizontal accuracy of each lidar data set. A systematic vertical misalignment between the two DTMs of 9.75 cm was also found that does not change the reach-scale patterns of erosion and deposition but can significantly affect the calculations of volumetric change across the landscape. While this value is within the reported vertical accuracy of the lidar data sets, this misalignment results in a 61.7% difference in the net volumetric change across the study area. When it can be quantified, it is possible to correct for a systematic error between two data sets to reduce the uncertainty in the DEM of Difference. Fully validating a vertical correction, however, would require extensive high-precision surveys of stable surfaces at the time of each lidar campaign to confirm their vertical alignment beyond the reported vertical uncertainty. These surveys are not available for the Rio Puerco; in their absence, much more extensive and precise ground-truthing of the flood deposit depths would be necessary to confirm the systematic error and its distribution across the landscape.

[73] The thickness of the 2006 flood deposits measured in the field represents a minimum depth of sediment accumulation during this event. The morphology of the deposits exposed within the pits revealed bed forms, scour features, and interbedded clay layers that suggest that the dynamics of the flow were spatially complex and evolved over time. The mismatch between the lidar differencing values and the field measurements is, in part, a consequence of the spatial variability of the patterns of deposition during the 2006 flood. Of the points collected at sites with sand-rich surface material, only 77% of the field measurements fall either within the vertical accuracy of the DoD at that specific point in the landscape (Figure 4, squares and black crosses) or are within one standard deviation of the differencing values within a 15 m radius (Figure 4, squares and dark gray bars). Field measurements from pits with clay-rich surface sediments (Figure 4, shaded) are consistently shallower than the change measured in the lidar differencing. Those pits are located in wide overbank channels between rows of tamarisk, and in unvegetated flats isolated from the primary down-valley flow. These topographically low zones often remain flooded following heavy rainfall and overbank flows. The clay-rich deposits seen in these pits might have settled out of suspension from standing water following the 2006 flood. Because of their grain size, we consistently miscategorized these post-flood deposits as pre-dating the 2006 event.

[74] The variability between the measurements collected in the field and seen in the DoD could also be the result of topographic change that occurred between the collection of the 2005 data set and the accumulation of the earliest preserved deposits of the 2006 flood, or between the 2010 lidar campaign and the 2011 field measurements. The USGS streamgage at Bernardo records several events in the month preceding the 2006 flood that could have caused minor overbank flooding and potentially affected surface morphology. Field observations suggest that floodplain erosion occurred along the study reach between March 2010 and November 2011, although the magnitude of topographic change cannot be quantified. Only one large event, in August 2005, was captured by the Bernardo streamgage during this period. Post-2006 sedimentation was observed, in November 2011, to be limited to 1 to 5 cm of unconsolidated sand on the surface.

6. Conclusions

[75] We present the results of an airborne lidar differencing study of the effects of a large flood on the topography of the Rio Puerco following the removal of vegetation from the floodplain and channel immediately upstream of the study area. The DEM of Difference (DoD) shows a net volumetric change of 578,050 $\pm \sim$ 490,000 m^3 across the study reach; 88.3% of the aggradation occurred along the floodplain and channel, while 76.7% of the erosion was focused along the vertical arroyo walls and terraces.

[76] At the coarse scale, the longitudinal variation in the depth of sedimentation along the arroyo bottom can be explained as the sum of two signals: an exponential depositional profile that decreases with distance from the devegetated reach, and the uniform deposition of locally sourced material. The sediment released from the sprayed reach only impacts the morphology of the arroyo bottom along the upstream 3.6 km of the study area. Further down-valley and elsewhere along the arroyo, widespread, uniform floodplain

aggradation is primarily the result of erosion of the arroyo walls through piping, gullying, and block collapse, and the flux of material from the upper valley surface.

[77] Superimposed on this down-valley trend are the finer-scale effects of vegetation and arroyo morphology on the routing of flow and sediment across the landscape. The depth of sedimentation within the arroyo bottom is weakly correlated with vegetation type and density. Aggradation is lowest in areas with minimal vegetation, while the highest depths of sedimentation generally occur where the landscape is 60–70% vegetated. The spatial variability in sedimentation depth is strongly correlated with vegetation type and density. The highest variability is observed within mature tamarisk, with thick, widely spaced stems. Uniform deposition thicknesses are seen when the floodplain is populated by sandbar willow and young tamarisk, with thin, closely spaced stems. While this study does not intend to discern the mechanisms that govern the interaction of flow, sediment, and vegetation, we suggest that the patterns of sediment distribution across the arroyo bottom are due to the nonlinear relationship between stem density and turbulence intensity [*Raupach*, 1992; *Nepf*, 1999; *Larsen et al.*, 2009; *Folkard*, 2011] that can lead to increased near-bed flow velocities and spatially varied shear stress within sparse vegetation and attenuated turbulence inside dense stem arrays. The reach-scale patterns of sedimentation observed through lidar differencing in this study likely reflect complex interactions of vegetation, flow, and sediment at the scale of patches to individual plants.

[78] The consequences of the 2006 flood on the Lower Rio Puerco accentuate the importance of developing and testing methods for assessing the hydrologic and sedimentary impacts of changes to riparian environments. The establishment and removal of plants from the landscape, as well as changes in the nature and density of the vegetation that could result from climate and land-use change, hold the potential to influence water quality and the health of ecosystems. Understanding the behavior of natural systems in response to these changes is fundamental for applying effective environmental management practices.

[79] **Acknowledgments.** The acquisition and processing of the 2010 lidar data was completed by the National Center for Airborne Laser Mapping (NCALM - http://www.ncalm.org). NCALM funding was provided by NSF's Division of Earth Sciences, Instrumentation and Facilities Program. EAR-1043051. http://dx.doi.org/10.5069/G9HT2M76. This work was supported by NSF grant EAR-1246546 to G.T. The Rocky Mountain Association of Geologists (RMAG) Foundation Bolyard Scholarship and the Cooperative Institute for Research in Environmental Sciences (CIRES) Graduate Student Research Fellowship provided support to M.P. We are grateful for field assistance from A. Langston, F. Rengers, and C. Walker. Finally, we thank two anonymous reviewers, A. Densmore, and P. Kinzel for constructive and helpful review comments. Any use of trade, firm, or product names is for descriptive purposes only and does not imply endorsement by the U.S. Government.

References

Abermann, J., A. Fischer, A. Lambrecht, and T. Geist (2009), Multitemporal airborne lidar-DEMs for glacier and permafrost mapping and monitoring, *The Cryosphere Discuss.*, *3*, 383–414, doi:10.5194/tcd-3-383-2009.

Abernethy, B., and I. Rutherfurd (2000), The effect of riparian tree roots on the mass-stability of riverbanks, *Earth Surf. Processes Landforms*, *25*(9), 921–937, doi:10.1002/1096-9837(200008)25:9<921::AID-ESP93>3.0.CO;2-7.

Afzalimehr, H., and S. Dey (2009), Influence of bank vegetation and gravel bed on velocity and Reynolds stress distributions, *Int. J. Sediment Res.*, *24*, 236–246, doi:10.1016/S1001-6279(09)60030-5.

Akca, D. (2010), Co-registration of surfaces by 3D least squares matching, *Photogramm. Eng. Remote Sens.*, *76*, 307–318.

Ashmore, P., and M. Church (1998), Sediment transport and river morphology: A paradigm for study, in *Gravel Bed Rivers in the Environment*, edited by P. Klingeman, R. Beschta, P. Komar, and J. Bradley, pp. 115–148, Water Resources Publications, Highlands Ranch, CO.

Bal, K., E. Struyf, H. Vereecken, P. Viaene, L. De Doncker, E. de Deckere, F. Mostaert, and P. Meire (2011), How do macrophyte distribution patterns affect hydraulic resistances?, *Ecol. Eng.*, *37*, 529–533, doi:10.1016/j.ecoleng.2010.12.018.

Barz, D., R. P. Watson, J. F. Kanney, J. D. Roberts, and D. P. Groeneveld (2009), Cost/benefit considerations for recent saltcedar control, Middle Pecos River, New Mexico, *Environ. Manage.*, *43*, 282–98, doi:10.1007/s00267-008-9156-9.

Beard, D., and P. Weyl (1973), Influence of texture on porosity and permeability of unconsolidated sand, *AAPG Bull.*, *57*(2), 349–369.

Bowen, Z., and R. Waltermire (2002), Evaluation of Light Detection and Ranging (LIDAR) for measuring river corridor topography, *J. Am. Water Resour. Assoc.*, *38*(1), 33–41, doi:10.1111/j.1752-1688.2002.tb01532.X.

Brasington, J., B. Rumsby, and R. McVey (2000), Monitoring and modelling morphological change in a braided gravel-bed river using high resolution GPS-based survey, *Earth Surf. Processes Landforms*, *25*(9), 973–990, doi:10.1002/1096-9837(200008)25:9<973::AID-ESP111>3.3.CO;2-P.

Bryan, K. (1925), Date of channel trenching (arroyo cutting) in the arid Southwest, *Science*, *62*(1607), 338, doi:10.1126/science.62.1607.338.

Bryan, K. (1928), Historic evidence on changes in the channel of Rio Puerco, a tributary of the Rio Grande in New Mexico, *The J. Geol.*, *36*(3), 265–282, doi:10.1086/623512.

Bryan, K., and G. Post (1927), Erosion and control of silt on the Rio Puerco, New Mexico, *Report to the Chief Engineer*, Middle Rio Grande Conservancy District, Albuquerque, NM.

Burns, W., J. Coe, B. Kaya, and L. Ma (2010), Analysis of elevation changes detected from multi-temporal lidar surveys in forested landslide terrain in western Oregon, *Environ. Eng. Geosci.*, *16*, 315–341, doi:10.2113/gseegeosci.16.4.315.

Burrough, P., and R. McDonnell (1998), *Principles of Geographical Information Systems*, Oxford University Press, Oxford, UK.

Celik, A., P. Diplas, C. Dancey, and M. Valyrakis (2010), Impulse and particle dislodgement under turbulent flow conditions, *Phys. Fluids*, *22*, 046,601, doi:10.1063/1.3385433.

Collins, K., and R. Ferrari (2000), Elephant Butte Reservoir, 1999 Sedimentation Survey, Sedimentation and River Hydraulics Group, *Tech. Rep.*, Technical Service Center, Bureau of Reclamation, Denver, CO.

Corenblit, D., and J. Steiger (2009), Vegetation as a major conductor of geomorphic changes on the Earth surface: Toward evolutionary geomorphology, *Earth Surf. Processes Landforms*, *34*, 891–896, doi:10.1002/esp.1788.

Corenblit, D., E. Tabacchi, J. Steiger, and A. Gurnell (2007), Reciprocal interactions and adjustments between fluvial landforms and vegetation dynamics in river corridors: A review of complementary approaches, *Earth Sci. Rev.*, *84*, 56–86, doi:10.1016/j.earscirev.2007.05.004.

Corsini, A., L. Borgatti, F. Coren, and M. Vellico (2007), Use of multitemporal airborne lidar surveys to analyse post-failure behaviour of earth slides, *Can. J. Remote Sens.*, *33*, 116–120, doi:10.5589/m07-015.

Coulthard, T. (2005), Effects of vegetation on braided stream pattern and dynamics, *Water Resour. Res.*, *41*, W04003, doi:10.1029/2004WR003201.

Davy, P., and D. Lague (2009), Fluvial erosion/transport equation of landscape evolution models revisited, *J. Geophys. Res.*, *114*, F03007, doi:10.1029/2008JF001146.

DeLong, S., C. Prentice, G. Hilley, and Y. Ebert (2011), Multitemporal ALSM change detection, sediment delivery, and process mapping at an active earthflow, *Earth Surf. Processes Landforms*, *37*, 262–272, doi:10.1002/esp.2234.

Dunkerley, D. (2008), Flow chutes in Fowlers Creek, arid western New South Wales, Australia: Evidence for diversity in the influence of trees on ephemeral channel form and process, *Geomorphology*, *102*, 232–241, doi:10.1016/j.geomorph.2008.05.004.

Elliott, J., A. Gellis, and S. Aby (1999), Evolution of arroyos: Incised channels of the southwestern United States, in *Incised River Channels*, edited by S. Darby, and A. Simon, pp. 153–185, John Wiley & Sons, New Jersey.

Favalli, M., A. Fornaciai, F. Mazzarini, A. Harris, M. Neri, B. Behncke, M. Pareschi, S. Tarquini, and E. Boschi (2010), Evolution of an active lava flow field using a multitemporal lidar acquisition, *J. Geophys. Res.*, *115*, B11203, doi:10.1029/2010JB007463.

Ferguson, R., and M. Church (2004), A simple universal equation for grain settling velocity, *J. Sediment. Res.*, *74*, 933–937, doi:10.1306/051204740933.

Filin, S. (2005), Elimination of systematic errors from airborne laser scanning data, in *Proceedings of the Geoscience and Remote Sensing Symposium,* vol. 1, pp. 517–520, IEEE, Seoul, South Korea, doi:10.1109/IGARSS.2005.1526225.

Finnigan, J. (2000), Turbulence in plant canopies, *Annu. Rev. Fluid Mech.*, *32*(1), 519–571, doi:10.1146/annurev.fluid.32.1.519.

Fisher, P., and N. Tate (2006), Causes and consequences of error in digital elevation models, *Prog. Phys. Geogr.*, *30*, 467–489, doi:10.1191/0309133306pp492ra.

Folkard, A. (2011), Flow regimes in gaps within stands of flexible vegetation: Laboratory flume simulations, *Environ. Fluid Mech.*, *11*, 289–306, doi:10.1007/s10652-010-9197-5.

Friedman, J., K. Vincent, and P. Shafroth (2005), Dating floodplain sediments using tree-ring response to burial, *Earth Surf. Processes Landforms*, *30*, 1077–1091, doi:10.1002/esp.1263.

Gellis, A., M. Pavich, and A. Ellwein (2001), Erosion and sediment yields in two subbasins of contrasting land use, Rio Puerco, New Mexico, in *Proceedings of the 7th Federal Interagency Sedimentation Conference* vol. 5, pp. 83-91, Subcommittee on Sedimentation, Reno, NV.

Gellis, A., M. Pavich, A. Ellwein, S. Aby, I. Clark, M. Wieczorek, and R. Viger (2011), Erosion, storage, and transport of sediment in two subbasins of the Rio Puerco, New Mexico, *Geol. Soc. Am. Bull.*, *124*(5-6), 817–841, doi:10.1130/B30392.1.

Graf, W. (1978), Fluvial adjustments to the spread of tamarisk in the Colorado Plateau region, *Geol. Soc. Am. Bull.*, *89*(10), 1491–1501, doi:10.1130/0016-7606(1978)89<1491:FATTSO>2.0.CO;2.

Green, J. (2005), Comparison of blockage factors in modelling the resistance of channels containing submerged macrophytes, *River Res. Appl.*, *21*, 671–686, doi:10.1002/rra.854.

Griffin, E., J. Smith, J. Friedman, and K. Vincent (2010), Progression of streambank erosion during a large flood, Rio Puerco Arroyo, New Mexico, in *Proceedings of the 2nd Joint Federal Interagency Conference*, 12 pp., Subcommittee on Sedimentation, Las Vegas, NV.

Griffin, E. G., J. Kean, K. Vincent, J. Smith, and J. Friedman (2005), Modeling effects of bank friction and woody bank vegetation on channel flow and boundary shear stress in the Rio Puerco, New Mexico, *J. Geophys. Res.*, *110*, F04023, doi:10.1029/2005JF000322.

Habib, A., A. Kersting, Z. Ruifang, M. Al-Durgham, C. Kim, and D. Lee (2008), Lidar strip adjustment using conjugate linear features in overlapping strips, *Int. Arch. Photogramm., Remote Sens. Spatial Inf. Sci.*, *37*(B1), 385-390.

Happ, S. (1948), Sedimentation in the Middle Rio Grande Valley, New Mexico, *Geol. Soc. Am. Bull.*, *59*(12), 1191–1218, doi:10.1130/0016-7606(1948)59[1191:SITMRG]2.0.CO;2.

Harvey, J., J. Pederson, and T. Rittenour (2011), Exploring relations between arroyo cycles and canyon paleoflood records in Buckskin Wash, Utah: Reconciling scientific paradigms, *Geol. Soc. Am. Bull.*, *123*, 2266–2276, doi:10.1130/B30374.1.

Heath, D. L. (1983), Flood and recharge relationships of the lower Rio Puerco, New Mexico, Master's thesis, New Mexico Institute of Mining and Technology, Socorro, NM.

Hodgson, M., and P. Bresnahan (2004), Accuracy of airborne lidar-derived elevation: Empirical assessment and error budget, *Photogramm. Eng. Remote Sens.*, *70*, 331–340.

Hooke, J. (2007), Monitoring morphological and vegetation changes and flow events in dryland river channels, *Environ. Monit. Assess.*, *127*, 445–457, doi:10.1007/s10661-006-9294-6.

Hopkinson, C., and M. Demuth (2006), Using airborne lidar to assess the influence of glacier downwasting on water resources in the Canadian Rocky Mountains, *Can. J. Remote Sens.*, *32*, 212–222, doi:10.5589/m06-012.

Hopkinson, L., and T. Wynn (2009), Vegetation impacts on near bank flow, *Ecohydrology*, *2*, 404–418, doi:10.1002/eco.87.

Hupp, C., and W. Osterkamp (1996), Riparian vegetation and fluvial geomorphic processes, *Geomorphology*, *14*(4), 277–295, doi:10.1016/0169-555X(95)00042-4.

Hutton, C., and R. Brazier (2012), Quantifying riparian zone structure from airborne lidar: Vegetation filtering, anisotropic interpolation, and uncertainty propagation, *J. Hydrol.*, *442–443*, 36–45, doi:10.1016/j.jhydrol.2012.03.043.

Istanbulluoglu, E., R. L. Bras, H. Flores-Cervantes, and G. E. Tucker (2005), Implications of bank failures and fluvial erosion for gully development: Field observations and modeling, *J. Geophys. Res.*, *110*, F01014, doi:10.1029/2004JF000145.

Jaeger, K., and E. Wohl (2011), Channel response in a semiarid stream to removal of tamarisk and Russian olive, *Water Resour. Res.*, *47*, W02536, doi:10.1029/2009WR008741.

Karlstrom, E., and T. Karlstrom (1987), Late Quaternary alluvial history of the American West: Toward a process paradigm, *Geology*, *15*(1), 88–89, doi:10.1130/0091-7613(1987)15<88:LQAHOT>2.0.CO;2.

Kean, J., and J. Smith (2006), Form drag in rivers due to small-scale natural topographic features: 2. Irregular sequences, *J. Geophys. Res.*, *111*, F04010, doi:10.1029/2006JF000490.

Kean, J. W., and J. D. Smith (2004), Flow and boundary shear stress in channels with woody bank vegetation, in *Riparian Vegetation and Fluvial Geomorphology*, edited by S. J. Bennett, and A. Simon, pp. 237–252, American Geophysical Union, Washington, D.C., doi:10.1029/008WSA17.

Kobler, A., N. Pfeifer, P. Ogrinc, L. Todorovski, K. Oštir, and S. Džeroski (2007), Repetitive interpolation: A robust algorithm for DTM generation from Aerial Laser Scanner Data in forested terrain, *Remote Sens. Environ.*, *108*, 9–23, doi:10.1016/j.rse.2006.10.013.

Kraus, K., C. Ressl, and A. Roncat (2006), Least squares matching for airborne laser scanner data, in *Proceedings of the 5th International Symposium Turkish-German Joint Geodetic Days "Geodesy and Geoinformation in the Service of our Daily Life,"* edited by L. Gründig, and O. Altan (eds.), 7 pp., Berlin, Germany.

Lane, S. (2003), The measurement of river channel morphology using digital photogrammetry, *The Photogramm. Rec.*, *16*(96), 937–961, doi:10.1111/0031-868X.00159.

Lane, S., K. Richards, and J. Chandler (1994), Developments in monitoring and modelling small-scale river bed topography, *Earth Surf. Processes Landforms*, *19*(4), 349–368, doi:10.1002/esp.3290190406.

Lane, S., R. Westaway, and D. Murray Hicks (2003), Estimation of erosion and deposition volumes in a large, gravel-bed, braided river using synoptic remote sensing, *Earth Surf. Processes Landforms*, *28*(3), 249–271, doi:10.1002/esp.483.

Larsen, L., J. Harvey, and J. Crimaldi (2009), Predicting bed shear stress and its role in sediment dynamics and restoration potential of the Everglades and other vegetated flow systems, *Ecol. Eng.*, *35*, 1773–1785, doi:10.1016/j.ecoleng.2009.09.002.

Lawson, S., K. McGlathery, and P. Wiberg (2012), Enhancement of sediment suspension and nutrient flux by benthic macrophytes at low biomass, *Mar. Ecol. Prog. Ser.*, *448*, 259–270, doi:10.3354/meps09579.

Legleiter, C., and P. Kyriakidis (2006), Forward and inverse transformations between cartesian and channel-fitted coordinate systems for meandering rivers, *Math. Geol.*, *38*, 927–958, doi:10.1007/s11004-006-9056-6.

Leopold, L. (1976), Reversal of erosion cycle and climatic change, *Quat. Res.*, *6*(4), 557–562, doi:10.1016/0033-5894(76)90026-0.

López, F., and M. García (1998), Open-channel flow through simulated vegetation: Suspended sediment transport modeling, *Water Resour. Res.*, *34*(9), 2341–2352, doi:10.1029/98WR01922.

Love, D. (1986), A geological perspective of sediment storage and delivery along the Rio Puerco, central New Mexico, in *Drainage Basin Sediment Delivery,* vol. 159, edited by R. Hadley, pp. 305–322, International Association of Hydrological Sciences Press, Wallingford, United Kingdom.

Luhar, M., and H. Nepf (2013), From the blade scale to the reach scale: A characterization of aquatic vegetative drag, *Adv. Water Res.*, *51*, 305-316, doi:10.1016/j.advwatres.2012.02.002.

Luhar, M., J. Rominger, and H. Nepf (2008), Interaction between flow, transport and vegetation spatial structure, *Environ. Fluid Mech.*, *8*, 423–439, doi:10.1007/s10652-008-9080-9.

Maas, H. (2000), Least-squares matching with airborne laser scanning data in a TIN structure, *Int. Arch. Photogramm. Remote Sens.*, *33*(3A), 548–555.

Maas, H. (2002), Methods for measuring height and planimetry discrepancies in airborne laser scanner data, *Photogramm. Eng. Remote Sens.*, *68*(9), 933–940.

MacEachren, A., and J. Davidson (1987), Sampling and isometric mapping of continuous geographic surfaces, *Cartogr. Geogr. Inf. Sci.*, *14*(4), 299–320, doi:10.1559/152304087783875723.

Maling, D. (1989), *Measurements From Maps: Principles and Methods of Cartometry*, Pergamon Press, New York, NY.

Matsuoka, A., T. Yamakoshi, K. Tamura, J. Maruyama, and K. Ogawa (2008), Sediment yield from seismically-disturbed mountainous watersheds revealed by multi-temporal aerial lidar surveys, *IAHS-AISH Publ.*, *325*, 208–216.

Meng, X., N. Currit, and K. Zhao (2010), Ground filtering algorithms for airborne lidar data: A review of critical issues, *Remote Sens.*, *2*, 833–860, doi:10.3390/rs2030833.

Micheli, E., and J. Kirchner (2002), Effects of wet meadow riparian vegetation on streambank erosion. 2. Measurements of vegetated bank strength and consequences for failure mechanics, *Earth Surf. Processes Landforms*, *27*(7), 687–697, doi:10.1002/esp.340.

Milne, J., and D. Sear (1997), Modelling river channel topography using GIS, *Int. J. Geogr. Inf. Sci.*, *11*(5), 499–519, doi:10.1080/136588197242275.

Mitasova, H., M. Overton, J. Recalde, D. Bernstein, and C. Freeman (2009), Raster-based analysis of coastal terrain dynamics from multitemporal lidar data, *J. Coastal Res.*, *25*, 507–514, doi:10.2112/07-0976.1.

Molnar, P., and J. Ramirez (2001), Recent trends in precipitation and streamflow in the Rio Puerco Basin, *J. Climate*, *14*(10), 2317–2328, doi:10.1175/1520-0442(2001)014<2317:RTIPAS>2.0.CO;2.

Moore, K. (2004), Influence of seagrasses on water quality in shallow regions of the lower Chesapeake Bay, *J. Coastal Res.*, *10045*, 162–178, doi:10.2112/SI45-162.1.

Murray, A., and C. Paola (2003), Modelling the effect of vegetation on channel pattern in bedload rivers, *Earth Surf. Processes Landforms*, *28*(2), 131–143, doi:10.1002/esp.428.

National Center for Airborne Laser Mapping (2011), Rio Puerco River, NM: Study of overbank flood dynamics, Houston, TX, doi:10.5069/G9ZW1HVC.

Nepf, H. (1999), Drag, turbulence, and diffusion in flow through emergent vegetation, *Water Resour. Res.*, *35*(2), 479–489, doi:10.1029/1998WR900069.

Nepf, H. (2012a), Flow and transport in regions with aquatic vegetation, *Annu. Rev. Fluid Mech.*, *44*, 123–142, doi:10.1146/annurev-fluid-120710-101048.

Nepf, H. (2012b), Hydrodynamics of vegetated channels, *J. Hydraul. Res.*, *50*, 262–279, doi:10.1080/00221686.2012.696559.

New Mexico Geospatial Data Acquisition Committee (2006), 2005 New Mexico DOQQs, State of New Mexico, Albuquerque, New Mexico, http://rgis.unm.edu/. Accessed 18 October 2006.

Nikora, V., S. Larned, N. Nikora, K. Debnath, G. Cooper, and M. Reid (2008), Hydraulic resistance due to aquatic vegetation in small streams: Field study, *J. Hydraul. Eng.*, *134*, 1326–1332, doi:10.1061/(ASCE)0733-9429(2008)134:9(1326).

Nordin, C. (1963), A preliminary study of sediment transport parameters, Rio Puerco near Bernado, New Mexico, *U.S. Geological Survey Professional Paper 462-C*, pp., U.S. Geological Survey, Washington, D.C.

Nordin, C., and W. Curtis (1962), Formation and deposition of clay balls, Rio Puerco, New Mexico, *U.S. Geological Survey Water-Resources Investigations Report, 28*, 37–40.

Osterkamp, W., and C. Hupp (2010), Fluvial processes and vegetation – Glimpses of the past, the present, and perhaps the future, *Geomorphology*, *116*, 274–285, doi:10.1016/j.geomorph.2009.11.018.

Phippen, S., and E. Wohl (2003), An assessment of land use and other factors affecting sediment loads in the Rio Puerco watershed, New Mexico, *Geomorphology*, *52*(3-4), 269–287, doi:10.1016/S0169-555X(02)00261-1.

Pollen-Bankhead, N., and A. Simon (2009), Enhanced application of root-reinforcement algorithms for bank-stability modeling, *Earth Surf. Processes Landforms*, *34*, 471–480, doi:10.1002/esp.1690.

Procter, J., S. Cronin, I. Fuller, G. Lube, and V. Manville (2010), Quantifying the geomorphic impacts of a lake-breakout lahar, Mount Ruapehu, New Zealand, *Geology*, *38*, 67, doi:10.1130/G30129.1.

Raupach, M. (1992), Drag and drag partition on rough surfaces, *Boundary-Layer Meteorol.*, *60*(4), 375–395, doi:10.1007/BF00155203.

Richards, J. (1986), *Remote Sensing Digital Image Analysis: An Introduction*, Springer-Verlag, Berlin.

Richter, A., D. Faust, and H. Maas (2011), Dune cliff erosion and beach width change at the northern and southern spits of Sylt detected with multi-temporal lidar, *Catena*, *103*, 103–111, doi:10.1016/j.catena.2011.02.007.

Rominger, J., and H. Nepf (2011), Flow adjustment and interior flow associated with a rectangular porous obstruction, *J. Fluid Mech.*, *680*, 636–659, doi:10.1017/jfm.2011.199.

Sallenger, A., C. Wright, K. Guy, and K. Morgan (2004), Assessing storm-induced damage and dune erosion using airborne lidar: Examples from Hurricane Isabel, *Shore & Beach*, *72*, 3–7.

Sandercock, P., J. Hooke, and J. Mant (2007), Vegetation in dryland river channels and its interaction with fluvial processes, *Prog. Phys. Geogr.*, *31*, 107–129, doi:10.1177/0309133307076106.

Schoneboom, T., J. Aberle, and A. Dittrich (2010), Hydraulic resistance of vegetated flows: Contribution of bed shear stress and vegetative drag to total hydraulic resistance, in *River Flow 2010: Proceedings of the International Conference on Fluvial Hydraulics River Flow*, edited by A. Dittrich, Ka. Koll, J. Aberle, and P. Geisenhainer, vol. 8, 269–276, Braunschweig, Germany.

Shafroth, P., J. Cleverly, T. Dudley, J. Taylor, C. Van Riper, E. Weeks, and J. Stuart (2005), Control of Tamarix in the Western United States: Implications for water salvage, wildlife use, and riparian restoration, *Environ. Manage.*, *35*, 231–246, doi:10.1007/s00267-004-0099-5.

Simon, A., and A. Collison (2002), Quantifying the mechanical and hydrologic effects of riparian vegetation on streambank stability, *Earth Surf. Processes Landforms*, *27*(5), 527–546, doi:10.1002/esp.325.

Simon, A., and R. Thomas (2002), Processes and forms of an unstable alluvial system with resistant, cohesive streambeds, *Earth Surf. Processes Landforms*, *27*(7), 699–718, doi:10.1002/esp.347.

Siniscalchi, F., V. Nikora, and J. Aberle (2012), Plant patch hydrodynamics in streams: Mean flow, turbulence, and drag forces, *Water Resour. Res.*, *48*, W01513, doi:10.1029/2011WR011050.

Smith, J. (2007), Beaver, willow shrubs, and floods, in *Plant Disturbance Ecology: The Process and the Response*, edited by E. Johnson, and K. Miyanishi, pp. 603–672, Elsevier Academic Press, Burlington, MA.

Smith, J., and E. Griffin (2002), Relation between geomorphic stability and the density of large shrubs on the flood plain of the Clark Fork of the Columbia River in the Deer Lodge Valley, Montana, *US Geological Survey Water-Resources Investigations Report*, pp. 02–4070.

Streutker, D., N. Glenn, and R. Shrestha (2011), A slope-based method for matching elevation surfaces, *Photogramm. Eng. Remote Sens.*, *77*, 743–750.

Stromsoe, N., and J. Callow (2012), The role of vegetation in mitigating the effects of landscape clearing upon dryland stream response trajectory and restoration potential, *Earth Surf. Processes Landforms*, *37*, 180–192, doi:10.1002/esp.2240.

Sukhodolov, A., and T. Sukhodolova (2010), Case study: Effect of submerged aquatic plants on turbulence structure in a lowland river, *J. Hydraul. Eng.*, *136*, 434–446, doi:10.1061/(ASCE)HY.1943-7900.0000195.

Tal, M., and C. Paola (2007), Dynamic single-thread channels maintained by the interaction of flow and vegetation, *Geology*, *35*, 347, doi:10.1130/G23260A.1.

Tanino, Y., and H. Nepf (2008), Lateral dispersion in random cylinder arrays at high Reynolds number, *J. Fluid Mech.*, *600*, 339–371, doi:10.1017/S0022112008000505.

Thorne, C. (1990), Effects of vegetation on riverbank erosion and stability, in *Vegetation and Erosion: Processes and Environments*, edited by J. B. Thornes, pp. 125–144, John Wiley & Sons, Chichester, England.

Thornthwaite, C., C. Sharpe, and E. Dosch (1942), Climate and accelerated erosion in the arid and semi-arid Southwest, with special reference to the Polacca Wash drainage basin, Arizona, *Tech. Rep. 808*, U.S. Department of Agriculture Technical Bulletin.

Tooth, S. (2000), Process, form and change in dryland rivers: A review of recent research, *Earth Sci. Rev.*, *51*(1), 67–107, doi:10.1016/S0012-8252(00)00014-3.

Tooth, S., and G. Nanson (2000), Equilibrium and nonequilibrium conditions in dryland rivers, *Phys. Geogr.*, *21*(3), 183–211.

Ventura, G., G. Vilardo, C. Terranova, and E. Sessa (2011), Tracking and evolution of complex active landslides by multi-temporal airborne lidar data: The Montaguto landslide (Southern Italy), *Remote Sens. Environ.*, *115*, 3237–3248, doi:10.1016/j.rse.2011.07.007.

Vincent, K., J. Friedman, and E. Griffin (2009), Erosional consequence of saltcedar control, *Environ. Manage.*, *44*, 218–227, doi:10.1007/s00267-009-9314-8.

Vollmer, S., and M. Kleinhans (2007), Predicting incipient motion, including the effect of turbulent pressure fluctuations in the bed, *Water Resour. Res.*, *43*, W05410, doi:10.1029/2006WR004919.

Waters, M. R., and C. V. Haynes (2001), Late Quaternary arroyo formation and climate change in the American Southwest, *Geology*, *29*(5), 399–402, doi:10.1130/0091-7613(2001)029<0399:LQAFAC>2.0.CO;2.

Westaway, R., S. Lane, and D. Hicks (2000), The development of an automated correction procedure for digital photogrammetry for the study of wide, shallow, gravel-bed rivers, *Earth Surf. Processes Landforms*, *25*(2), 209–226, doi:10.1002/(SICI)1096-9837(200002)25:2<209::AID-ESP84>3.0.CO;2-Z.

Westaway, R., S. Lane, and D. Hicks (2003), Remote survey of large-scale braided, gravel-bed rivers using digital photogrammetry and image analysis, *Int. J. Remote Sens.*, *24*(4), 795–815, doi:10.1080/01431160110113070.

Wheaton, J. (2008), Uncertainty in morphological sediment budgeting of rivers, Ph.D. thesis, University of Southampton, Southampton, UK.

Wheaton, J., J. Brasington, S. Darby, and D. Sear (2010), Accounting for uncertainty in DEMs from repeat topographic surveys: Improved sediment budgets, *Earth Surf. Processes Landforms*, *35*, 136–156, doi:10.1002/esp.1886.

Wheaton, J., J. Brasington, S. Darby, A. Kasprak, D. Sear, and D. Vericat (2013), Morphodynamic signatures of braiding mechanisms as expressed through change in sediment storage in a gravel-bed river, *J. Geophys. Res. Earth Surf.*, doi:10.1002/jgrf.20060.

White, S., and Y. Wang (2003), Utilizing DEMs derived from lidar data to analyze morphologic change in the North Carolina coastline, *Remote Sens. Environ.*, *85*(1), 39–47, doi:10.1016/S0034-4257(02)00185-2.

Winterbottom, S., and D. Gilvear (1997), Quantification of channel bed morphology in gravel-bed rivers using airborne multispectral imagery and aerial photography, *Regul. Rivers: Res. & Manage.*, *13*(6), 489–499, doi:10.1002/(SICI)1099-1646(199711/12)13:6<489::AID-RRR471>3.0.CO;2-X.

Wise, S. (2000), Assessing the quality for hydrological applications of digital elevation models derived from contours, *Hydrol. Processes*, *14*(11-12), 1909–1929, doi:10.1002/1099-1085(20000815/30)14:11/12<1909::AID-HYP45>3.0.CO;2-6.

Woolard, J., and J. Colby (2002), Spatial characterization, resolution, and volumetric change of coastal dunes using airborne lidar: Cape Hatteras, North Carolina, *Geomorphology*, *48*(1), 269–287, doi:10.1016/S0169-555X(02)00185-X.

Zhang, K., and D. Whitman (2005), Comparison of three algorithms for filtering airborne lidar data, *Photogramm. Eng. Remote Sens.*, *71*, 313–324.

Zong, L., and H. Nepf (2010), Flow and deposition in and around a finite patch of vegetation, *Geomorphology*, *116*, 363–372, doi:10.1016/j.geomorph.2009.11.020.

Zong, L., and H. Nepf (2011), Spatial distribution of deposition within a patch of vegetation, *Water Resour. Res.*, *47*, W03516, doi:10.1029/2010WR009516.